Review of the temporal stability of the magnetic field for ultra-high field superconducting magnets with a particular focus on superconducting joints between HTS conductors

Y Takeda[1], H Maeda[2,3], K Ohki[4] and Y Yanagisawa[3]

[1] National Institute for Materials Science, 3-13 Sakura, Tsukuba, Ibaraki 305-0003, Japan
[2] Japan Science and Technology Agency, Kawaguchi, Saitama 332-0012, Japan
[3] RIKEN Center for Biosystems Dynamics Research, 1-7-22 Suehiro-cho, Tsurumi-ku, Yokohama 230-0045, Japan
[4] Sumitomo Electric Industries, Ltd., 1-1-3, Shimaya, Konohana-ku, Osaka, 554-0024, Japan

E-mail: TAKEDA.Yasuaki@nims.go.jp

Received xxxxxx
Accepted for publication xxxxxx
Published xxxxxx

Abstract

Superconducting magnets used in applications such as magnetic resonance imaging (MRI) and nuclear magnetic resonance (NMR) require significant temporal magnetic field stability, which can be achieved when the MRI and NMR magnets are operated in the persistent current mode (persistent-mode) using superconducting joints. However, the ultra-high field MRI and NMR magnets are sometimes operated in the driven mode. Herein, we present an analysis of the temporal magnetic field drift and fluctuations observed for MRI and NMR magnets operating in the driven mode and an exploration of effective methods for stabilizing the temporal magnetic field fluctuations. In the last decade, substantial improvements have been achieved in superconducting joints between high-temperature superconductors (HTS). These superconducting joints enable the development of persistent-mode ultra-high field magnets using HTS coils. Therefore, we herein review the superconducting joint technology for HTS conductors and describe the results of the persistent-mode operation achieved by a medium-field NMR magnet using an HTS coil. Particularly, the cutting-edge progress achieved concerning HTS superconducting joints, including joining methods, superconducting properties, and future prospects, is highlighted along with the issues that need to be addressed.

Keywords: ultra-high field magnets, temporal stability, persistent current mode, HTS, superconducting joint

1. Introduction

Superconducting magnets are widely used in applications such as magnetic resonance imaging (MRI), nuclear magnetic resonance (NMR), magnetically levitated trains, accelerators, fusion reactors, and high field research magnets. Among these, the ones used in MRI are the largest and highest powered commercially available superconducting magnets with a

market value of over 3 billion €/a [1]. Superconducting magnets for MRI and NMR require sufficient temporal magnetic field stability and spacial magnetic field homogeneity for applications in medical imaging and NMR spectroscopy.

The necessary temporal field stability required for MRI and NMR magnets is 100 ppb/h and < 10 ppb/h, respectively. However, the temporal field stability of NMR magnets can be further stabilized to < 1 ppb using an internal ^{2}H field-frequency lock system installed in the spectrometer [2]. Therefore, MRI and NMR magnets are usually operated in a persistent current mode (persistent-mode), using superconducting joints, with a resistance of less than 10^{-13} Ω [3][4][5].

After the commercialization of NMR spectrometers in the 1950s, iron-core electromagnets were used as NMR magnets with a maximum magnetic field intensity limit of 2.35 T (100 MHz for ^{1}H NMR) owing to the magnetic saturation of the iron-core [6]. As the sensitivity and resolution of NMR spectra depend on the magnetic field intensity, superconducting magnets were used along with Nb-based low-temperature superconductor (LTS) wires in the 1960s [6][7]. The first superconducting NMR magnet was developed in the US for a 4.7 T (200 MHz) NMR system using an NbZr single filament wire [8]. The magnet was operated in the persistent-mode, which required key technologies such as superconducting joints between superconducting wires and a superconducting switch. A US patent [9] demonstrated the fabrication process for a superconducting joint, wherein a twisted pair of NbZr wires and a metal sleeve were cold-pressed together to form a joint. Moreover, they achieved magnetic field stability of 10 ppb/h, which was further stabilized using an internal ^{2}H field-frequency lock system. However, the NbZr conductor was gradually replaced by multifilamentary NbTi conductors that exhibited higher ductility and better superconducting properties at high magnetic fields. In the 1970s, a persistent-mode 9.4 T (400 MHz) NMR magnet was realized using a superconducting joint described before [10]. Furthermore, the multifilamentary NbTi conductor with a CuNi matrix was used to form a superconducting switch required for demonstrating a persistent-mode operation. The persistent-mode NbTi magnet technology described thus far has been used in the commercial whole-body MRI magnets having a magnetic field range of up to 3 T [11].

A Nb_3Sn inner coil is necessary to further enhance the magnetic field of NMR magnets as upper critical field (B_{c2}) for the Nb_3Sn conductor can be as high as 25 T at 4.2 K [12]. However, because the Nb_3Sn conductor is brittle, it is impossible to form a cold-pressed superconducting joint. Therefore, in the 1980s, an indirect superconducting joint with a superconducting solder was developed using Thornton's matrix-replacement technique [13]. The Cu matrix of the conductor was replaced with Sn, which in turn was substituted with a superconducting solder. Then, the Nb_3Sn or NbTi filaments were coated with the superconducting solder and bonded together, resulting in a persistent-mode NMR magnet with a magnetic field of 11.75 T (500 MHz) [6]. In the 2000s, Bruker achieved a maximum magnetic field of 23.5 T (1 GHz) [14], which is a world record of the persistent-mode LTS NMR magnets.

However, the critical current density (J_c) of the Nb_3Sn conductor is insufficient above 23.5 T (1 GHz) at 1.9 K [15]. Therefore, a high-temperature superconductor (HTS) inner coil is crucial for generating ultra-high magnetic fields beyond ~23 T. The three representative HTS conductors are $REBa_2Cu_3O_y$ (REBCO, RE is rare earth, critical temperature $T_c \approx 90$ K), $(Bi,Pb)_2Sr_2Ca_2Cu_3O_y$ (Bi-2223, $T_c \approx 110$ K), and $Bi_2Sr_2CaCu_2O_y$ (Bi-2212, $T_c < 95$ K) [15][16]. Manufacturing companies produce sufficiently long practical conductors with a high J_c. Several research institutes have generated ultra-high magnetic fields beyond 30 T using an LTS/HTS magnet containing an HTS inner coil and an LTS outer coil [17][18][19].

Realizing a persistent-mode operation in an LTS/HTS NMR magnet is a considerable challenge owing to the complexity of the superconducting joint for HTS conductors. Therefore, to achieve an ultra-high field NMR magnet operating at > 23.5 T, Yanagisawa et al. developed a driven mode LTS/HTS 11.75 T (500 MHz) NMR magnet [20]. Although the generated magnetic field exhibited ripples and drifts over time depending on the performance of the power supply, they demonstrated the possibility of stabilizing the magnetic field using a highly stable current supply and a field-frequency lock system [21]. Subsequently, Hashi et al. succeeded in developing a 24 T (1.02 GHz) driven mode NMR magnet and acquired NMR spectra of biological samples [22][23]. Furthermore, MIT is developing a 30.5 T (1.3 GHz) driven mode NMR magnet [24]. Although it is possible to obtain excellent NMR spectra, the driven mode NMR magnet has certain limitations such as a complex magnet operation, excessive He consumption, and operation failure during power outage. Therefore, the persistent-mode operation is preferred.

In 2013, Lee et al [25] and Park et al. [26][27][28] overcame these shortcomings by introducing a superconducting joint between the REBCO conductors using a direct-type joining method. However, this method exhibited insufficient robustness against mechanical stress. In the following years, the authors successfully developed indirect-type superconducting joints between REBCO conductors [29] and Bi-2223 conductors [30] by introducing an intermediate superconducting layer between a couple of the HTS conductors. The critical current (I_c) and mechanical properties were sufficient, and the joint resistance was less than 10^{-12} Ω. Our group then produced a 9.39 T (400 MHz) LTS/REBCO

NMR magnet with superconducting joints [31]. Furthermore, we commenced the Mirai Program funded by the Japan Science and Technology Agency (JST) to develop a persistent-mode 30.5 T (1.3 GHz) LTS/HTS NMR magnet comprising a REBCO inner coil, a Bi-2223 middle coil, and LTS outer coils. The HTS conductors are joined together with the superconducting joints [32].

Bruker-BioSpin GmbH in the EU recently developed and commercialized a persistent-mode 28.2 T (1.2 GHz) LTS/REBCO NMR magnet [33]. However, they did not reveal whether superconducting joints or solder lap joints were installed between the HTS and NbTi conductors as described in their patent [34]. Nevertheless, the NMR magnet achieved sufficient magnetic field stability for multidimensional NMR measurements.

Considering that the target magnetic field intensity of MRI and NMR magnets has been recently enhanced, the production methods of these magnets differ from those of the traditional persistent-mode magnets. For example, an 11.75 T (500 MHz) whole-body MRI magnet, comprising a fully stabilized NbTi main-coil and high-current density NbTi shielding coils, is being developed by NEUROSPIN of CEA Saclay in France for studying the human brain [35]. Because of the large size of the magnet (weighing 132 tons) and a high operating current (1500 A), the persistent-mode operation was not feasible; consequently, the magnet was operated in the driven mode. Owing to a small resistance connected in parallel with the MRI magnet, a temporally stabilized magnetic field sufficient for MR imaging was achieved.

Another example is a 35.25 T (1.5 GHz) hybrid NMR magnet comprising a water-cooled inner magnet and a cable-in-conduit outer magnet connected in series and operated simultaneously in the driven mode. The fluctuations in the magnetic field of the prototype magnet were regulated within 200 ppb using an external field-frequency lock system applicable to solid-state NMR measurements [36][37].

This paper provides an overview of *the temporal magnetic field stability* for NMR and MRI magnets. Section 2 explains the temporal magnetic field drift and fluctuations in NMR and MRI magnets operated in the driven mode, and effective methods to stabilize them. Furthermore, we refer to the field stabilization methods applied to the 11.75 T (500 MHz) MRI and 35.25 T (1.5 GHz) NMR magnets. Section 3 reviews the development of superconducting joints between the REBCO, Bi-2223, and Bi-2212 conductors. Major improvements have been achieved in the superconducting joint technology for developing joints between HTS conductors after reviewing the persistent joint reported by Brittles et al. [3] in 2015. Particularly, the recent progress and prospect of HTS superconducting joints are discussed. Furthermore, we discuss the 9.39 T (400 MHz) LTS/REBCO persistent-mode NMR magnet with REBCO superconducting joints, which has been under operation for over two years.

2. Temporal fluctuations and stabilization of the magnetic field for NMR and MRI magnets

2.1 Magnetic field fluctuation for NMR magnets operated in the driven mode

Yanagisawa et al. operated an 11.75 T LTS/Bi-2223 NMR magnet (500 MHz for ^{1}H NMR) in the driven mode [20] using an ultra-high-stabilized external DC power supply (~1 ppm). The LTS outer coil and the Bi-2223 inner coil were connected in series and charged simultaneously. Figure 1 shows the temporal drifts over 115 h after the magnet was charged. The magnetic field increased with time at a rate of 19 ppm/h and saturated at 50 ppb/h, which was a five-fold increase compared to the specifications of the NMR magnet (10 ppb/h). The inset in Figure 1 indicates that as the deviation in the magnetic field varied linearly with logarithmic time, the relaxation of the screening current dominated the temporal magnetic field drift. If the coil current is reversed by a significant value at a peak current, the positive drift of the magnetic field reduces significantly (current sweep reversal method), as indicated by the dashed blue line in Figure 1.

Figure 2 shows a magnified view of the fluctuations in the temporal magnetic field 20 days after the magnet was charged [20]. The field fluctuation comprised three components as described below:

(a) Long-term magnetic field drift [38]: Owing to the relaxation of the screening current-induced magnetic field in the Bi-2223 inner coil, the long-term magnetic field drifted at a rate of 10 ppb/h, which coincides with the extrapolated line shown in the inset in Figure 1. Although the long-term magnetic field drift can be reduced using the current sweep reversal method, it can also be enhanced further by using a REBCO insert coil because the screening current effect is more significant for the REBCO insert coil than for the Bi-2223 insert coil [39]. For ultra-high field NMR magnets, as the screening current-induced magnetic field decreases with an increase in the magnetic field intensity, the magnetic field drift reduces.

(b) Short-term magnetic field ripples: Short-term magnetic field ripples are caused by the DC power supply and exhibit a peak–peak amplitude of 0.2 ppm (200 ppb). Figure 3 shows a magnified view of the short-term magnetic field fluctuations for an 11.75 T (500 MHz) LTS NMR magnet operated in the driven mode. The vertical axis indicates the magnet current derived from the coil voltage instead of the magnetic field [21]. The magnet current fluctuates irregularly with a peak–peak amplitude of 0.45 ppm, a field fluctuation component of 0.003–0.005 Hz (Figure 3(a)), and field waves of ~2 and 50 Hz (Figure 3(b)). The amplitude of the magnetic field

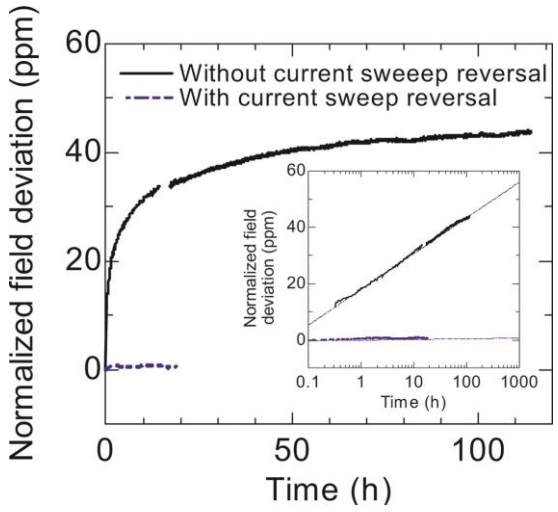

Figure 1. Temporal drift of the magnetic field for the driven mode 11.75 T LTS/Bi-2223 NMR magnet after the magnet was charged. The positive drift was reduced using the current sweep reversal method, as shown by the dashed blue line. Figure adapted from [20]. (Elsevier, 2010).

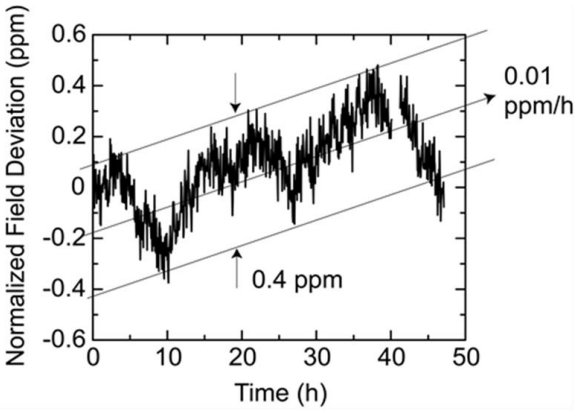

Figure 2. Magnified temporal magnetic field fluctuations 20 days after the magnet was charged. The field fluctuation comprised three components such as long-term magnetic field drift, short-term magnetic field ripples, and daily variations of the magnetic field. Figure adapted from [20]. (Elsevier, 2010).

ripple depends on the performance of the DC power supply and decreases on using a highly stabilized DC power supply. (c) Daily variation in the magnetic field: The daily variations in the magnetic field, exhibiting a peak–peak amplitude of 0.4 ppm (400 ppb), occur owing to the daily variations in the temperatures of the magnet site and environment, as well as the coolant of the DC power supply. The magnitude of the

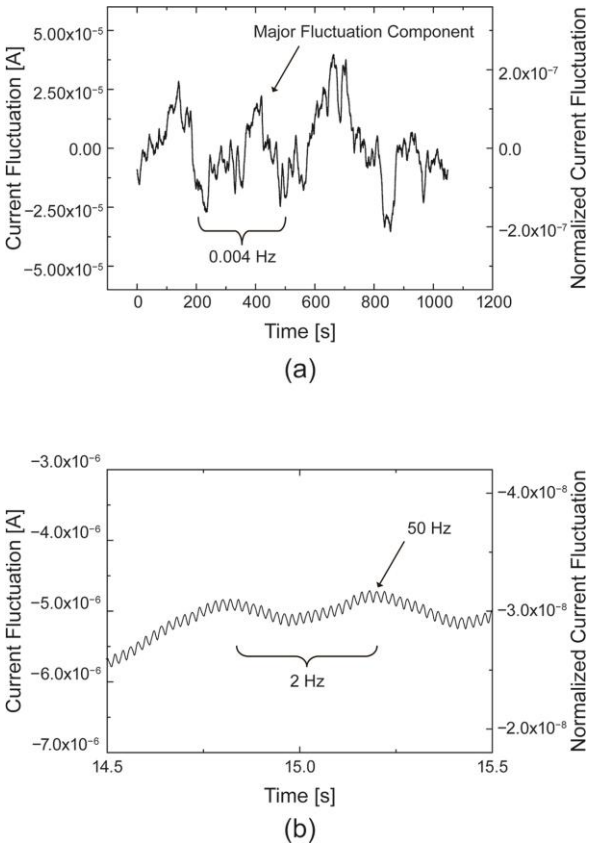

Figure 3. Magnetic field fluctuations of the 11.75 T LTS NMR magnet: The coil current changes irregularly, with a peak-peak amplitude of 0.45 ppm, comprising field ripples of 0.003–0.005, ~2, and 50 Hz. Figure adapted from [21] (Elsevier, 2008).

field variation depends on the installation conditions of the NMR magnet and the DC power supply.

The specifications necessary for the high-resolution solution and high-resolution solid-state NMR are < 1 ppb and 100 ppb, respectively. Therefore, the aforementioned magnetic field fluctuations are too large to perform high-resolution NMR measurements. This can be a major drawback when performing multidimensional NMR measurements as numerous T_1 noises appear in the vertical direction on the NMR spectrum. Therefore, it is necessary to stabilize the fluctuations in the magnetic field of NMR magnets operated in the driven mode.

2. 2 Stabilizing NMR and MRI magnets operated in the driven mode

2.2.1 Field-frequency lock system. The most straightforward approach to stabilize the temporal magnetic field fluctuations in an NMR magnet is to install a field-frequency lock system in the NMR system [2]. The stabilized

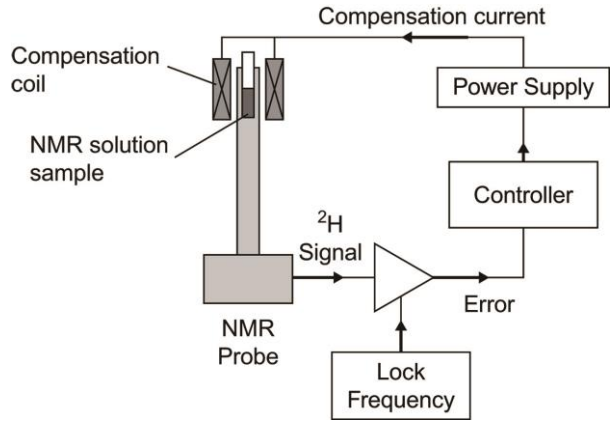

Figure 4. Schematic drawing of the internal field-frequency lock system for detecting the NMR peak of ^{2}H nuclei by controlling the compensation coil current. Figure modified from [21] (Elsevier, 2008)

magnetic field is limited to a 5 mm wide and 15 mm long NMR sample tube, whereas the NMR magnet bore has a diameter of 54 mm. Figure 4 shows the internal field-frequency lock system, which is modified from the image presented in [21]. The system continuously measures the ^{2}H nuclei NMR signal included in the NMR sample. If the peak frequency of the ^{2}H NMR signal deviates from the lock frequency, the controlling system provides a current to the compensation coil. The lock system can compensate for noises < 10 Hz, if adequate feedback loop parameters are chosen [21], which can help to compensate for the long-term magnetic field drift, short-term magnetic field ripples, and daily variations of the magnetic field. However, no compensation can be made for the 50 Hz noise, which exceeds the cut off-frequency of the lock controlling system.

Figure 5 shows examples of the field compensation effect of the internal field-frequency lock system for the 11.75 T LTS NMR magnet (500 MHz for ^{1}H NMR) operated in the driven mode [21], indicating a temporal change in the NMR spectra for 1% $CHCl_3$ in acetone-d6. Figure 5(a) shows the case without the field-frequency lock operation. The spectral peak changes irregularly with an amplitude of 0.34 ppm, thereby modulating the NMR spectrum shape. Conversely, if the field-frequency lock system is operated, the peak frequency deviation decreases to < 1 ppb, as evident in Figure 5(b). Therefore, the internal field-frequency lock system can effectively stabilize the magnetic field fluctuations for performing high-resolution NMR measurements. In contrast, an internal field-frequency lock system cannot be used for solid-state NMR measurements. The magnetic field fluctuation is stabilized to 20 ppb, if an external field-frequency lock system is used [40].

Magnetic field homogeneity is necessary for operating the field-frequency lock system. Considering that the upper limit

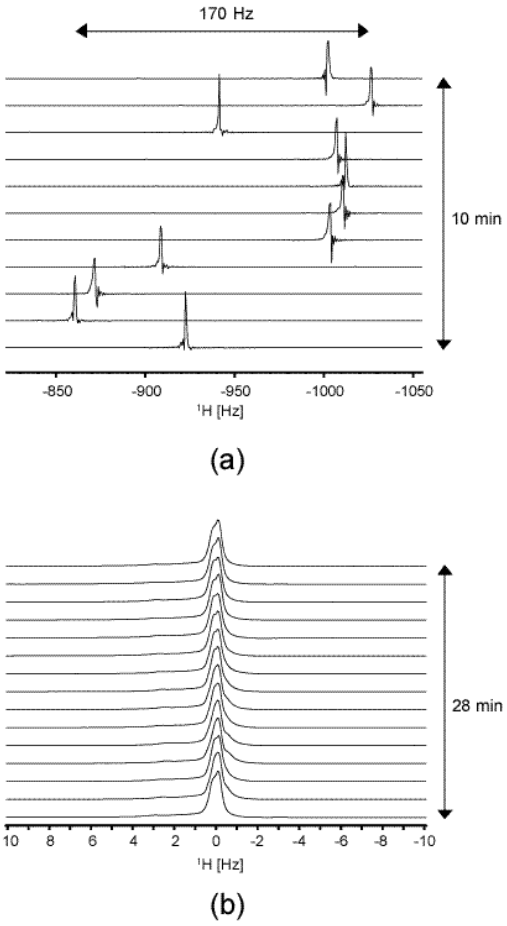

Figure 5. Examples of the compensation effect of the internal field-frequency lock system for the driven mode 11.75 T LTS NMR magnet: (a) Without the lock operation, and (b) with the lock operation. Figure adapted from [21] (Elsevier, 2008).

for the field-frequency lock operation is ±1–2 ppm [20][21], if the long-term magnetic field drift is 10 ppb/h, the available acquisition time of the NMR would be 100–200 h, which is sufficient for performing multidimensional NMR measurements. This defines the 10 ppb/h specification of the NMR magnet.

2.2.2 Temporal stabilization of the ultra-high magnetic field of the LTS/Bi-2223 NMR magnet operated in the driven mode. Thus far, we have described the temporal magnetic field fluctuations of a medium-field NMR magnet. Herein, we analyze the results achieved for a 24 T (1.02 GHz) LTS/Bi-2223 NMR magnet operated in the driven mode [22][23]. Figure 6(a) shows the magnetic field fluctuation at 24 T without the internal field-frequency lock system. The peak–peak amplitude of the short-term ripples is 0.4 ppm, similar to that shown in Figure 2. Furthermore, the daily

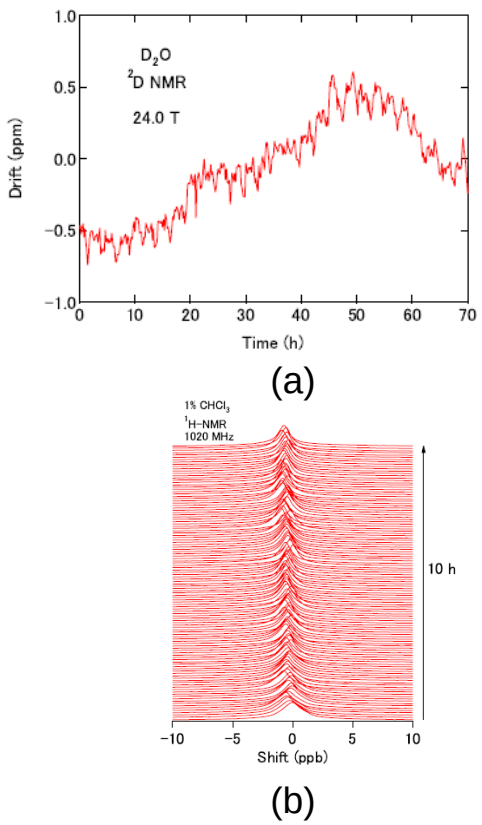

Figure 6. Magnetic field fluctuation for a driven mode 24 T LTS/Bi-2223 NMR magnet: (a) without the lock operation and (b) with the lock operation. Figure adapted from [22] (Elsevier, 2015).

variation of the magnetic field is ~1 ppm, which is twice of that shown in Figure 2. Compared to Figure 1, the long-term magnetic field drifts are not remarkable after the coil is charged because of the screening current effect, which significantly reduces under ultra-high magnetic fields of 20 T. As shown in Figure 6(b), an internal field-frequency lock system stabilizes the temporal magnetic field fluctuation at 1 ppb. Therefore, we achieved excellent multidimensional solution NMR and solid-state NMR using the 24 T LTS/Bi-2223 NMR system [23].

2.2.3 Temporal stabilization of the ultra-high magnetic field of a hybrid NMR magnet operated in the driven mode. The NHMFL, USA, developed a 35.2 T hybrid NMR magnet (1.5 GHz) operated in the driven mode, comprising a water-cooled resistive inner magnet (22.2 T) and a cable-in-conduit Nb_3Sn outer magnet (13 T) connected in series and simultaneously charged to 20 kA [36][37]. Both the ferromagnetic shims and resistive shim coils were installed inside the bore at room temperature. The increase in the magnet inductance significantly reduced the 60-Hz magnetic field ripples of the DC power supply [36]. Furthermore, the external field-frequency lock system with Li nuclei stabilized the magnetic field fluctuations. Figure 7(a) and 7(b) show the temporal fluctuations in the magnetic field achieved without and with the field-frequency lock operation, respectively [36]. The field-frequency lock operation presently reduces the magnetic fluctuations within 0.2 ppm, thereby obtaining excellent high-resolution multidimensional NMR spectra of quadrupolar nuclei in solid materials and solid proteins successfully.

2.2.4 Temporal stabilization of the ultra-high magnetic field of an MRI magnet. The maximum magnetic field available for commercial MRI magnets used in clinical purpose is 3 T. Because the imaging sensitivity and resolution depend on the intensity of the magnetic field, higher magnetic fields are preferred. To date, multiple 7 T MRI magnet systems have been developed for medical research, and several 9.4 T MRI magnet systems, also known as persistent-mode NbTi magnets, are being developed [11].

CEA Saclay, France, is developing an 11.75 T whole-body Bi-2223 MRI magnet for brain imaging [35]. Because ultra-high field MRI magnets exhibit magnetic quenches during their operation because of the interaction between the MRI magnet and the gradient coils, the 11.75 T MRI magnet comprises a fully stabilized main magnet along with epoxy impregnated shielding magnets to eliminate the magnet quenches. The magnet is operated in the driven mode, because of its operation current, i.e., 1500 A, making it impossible for the magnet to operate in the persistent-mode. The temporal magnetic field stability of the 11.75 T MRI magnet is ±0.05 ppm/h, which is lower than the current stability for the highly stabilized DC power supply. For example, the short-term magnetic field fluctuations and daily variations in the magnetic field are ±0.2 ppm, as depicted in Figure 2. The field-frequency lock system is unavailable for the 11.75 T MRI magnet because the magnetic field must be stabilized over a large spherical volume (sphere diameter: 22 cm). Therefore, an ultra-low resistance filtering resistor (e.g., 100 μΩ) and a fault-current-limiter (FCL) are combined and connected in parallel to the MRI magnet and the DC power supply. The FCL is used to protect the magnet from magnet quenches. The short-term ripples (e.g., the 2 and 50 Hz ripples seen in Figure 3) and longer-term fluctuations flow to the filtering resistance and the magnet, respectively. The magnetic field of the magnet has been successfully stabilized to ~0.1 ppm in the driven mode [35].

2.2.5 Medium-field HTS MRI magnets operated in the driven mode. Terao et al. [41] developed a He-free 3 T MRI magnet operated at 10–20 K using Bi-2223 conductors for brain imaging. The bore diameter of the magnet was 514 mm at room temperature, and was operated in the driven mode

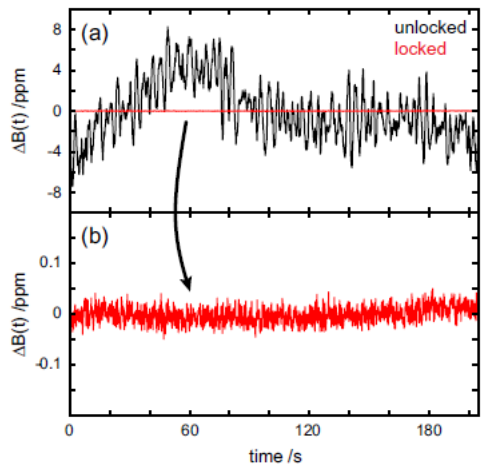

Figure 7. Temporal fluctuation of the magnetic field for a series connected 35.2 T hybrid magnet achieved without and with the external field-frequency lock operation. Figure adapted from [36] (Elsevier, 2017).

with an ultra-high-stabilized DC power supply. A long-term positive drift rate of < 1 ppm/h was observed owing to the screening current-induced magnetic field at 1.5 T. When the current sweep reversal was applied by 1%, the long-term drift rate reduced ten-fold to < −1 ppm/15 h, which was sufficient for brain imaging. The short-term ripples of the magnetic field were not considered.

Yokoyama et al. [42] developed a half-sized He-free active shield-type 3 T whole-body MRI magnet with a bore diameter of 480 mm at room temperature using REBCO conductors, and operated the device in the driven mode [43]. The temporal magnetic field drift due to the screening current was significant because of the REBCO conductors. Therefore, an additional DC power supply was used to compensate for the long-term drift associated with the screening current. This reduced the long-term magnetic field drift from 7.14 to 0.57 ppm/h, which was sufficient for MRI measurements.

2.3 *Temporal drift and stabilization of the magnetic field achieved for NMR magnets operated in the persistent-mode*

2.3.1 Persistent-mode ultra-high field LTS NMR magnet. Persistent-mode superconducting magnets are preferred over the driven mode magnets for achieving a temporally stabilized magnetic field. LTS conductors such as NbTi and Nb_3Sn, which are used in the LTS NMR and MRI persistent-mode magnets, are connected by superconducting joints having a joint resistance (R_j) of less than 10^{-13} Ω [3]. As aforedescribed, the cold-pressed and matrix-replacement methods, which are mature technologies for NMR manufacturers, are usually used for the NbTi [9] and Nb_3Sn conductors [13], respectively. Figure 8 demonstrates an example of an ultra-high field 21.6 T persistent-mode LTS NMR magnet (920 MHz for ^{1}H NMR)[44][45]. The magnet is cooled at < 2 K using subcooled superfluid He, resulting in a long-term drift rate of −0.336 ppb/h, which is thirty-fold lower than the usual specification of the NMR magnets (10 ppb/h). Furthermore, the field drift rate corresponds to the circuit resistance of 10^{-10} Ω. The magnetic field can be stabilized further to 0.01 ppb using the field-frequency lock system installed in the NMR spectrometer.

2.3.2 Design of a 30.5 T (1.3 GHz) persistent-mode ultra-high field LTS/HTS NMR magnet. Owing to the difficulties in producing practical superconducting joints between HTS conductors, only a few persistent-mode LTS/HTS magnets have been successfully developed. In 2017, a Japanese team, which included the authors of this paper, began developing a 30.5 T (1.3 GHz) LTS/HTS NMR persistent-mode magnet as a part of the Mirai Program supported by the JST [32], which will be completed in 2024. The magnet comprises a REBCO inner coil, a Bi-2223 middle coil, and LTS outer coils connected in series. The NbTi persistent current switch is connected in parallel to the magnet, and the coils are cooled using liquid He at 4.2 K. The HTS and LTS coils generate magnetic fields of 15.5 and 15 T, respectively. Superconducting joints between the HTS conductors are still being developed. Given below is a brief description of this 30.5 T magnet as a representative for ultra-high field persistent-mode NMR magnets.

Given that the total inductance of an NMR magnet is 960 H, the permissible circuit resistance would be < 10 ppb/h, which corresponds to $< 3 \times 10^{-9}$ Ω. The resistance comprises three parts:

(1) Resistance for the LTS outer coils: Considering that the inductance of the LTS coil is 836 H, the joint resistance corresponding to 10 ppb/h is $< 2.5 \times 10^{-9}$ Ω. It is essential to achieve a low resistance of 10^{-10} Ω, as seen in Figure 8, because the outer magnet of the 30.5 T magnet is cooled using liquid He (4.2 K) instead of superfluid He (< 2 K).

(2) Joint resistance between LTS and HTS: Developing a superconducting joint between HTS and LTS is highly challenging (described later in this paper). Therefore, the joint has a resistance of ~10^{-10} Ω, corresponding to the total resistance of 4×10^{-10} Ω.

(3) Joint resistance between HTS conductors: Since the total number of joints between the HTS conductors in the magnet is ~100, the individual R_j must be $< 10^{-12}$ Ω, which results in a total joint resistance of $< 10^{-10}$ Ω. The coil operating current for the magnet is ~200 A. We can estimate the required I_c of the joints for achieving an R_j of 10^{-12} Ω at 200 A using the power-*n* model, assuming that the model is correct in the ultra-low voltage region. If *n* =

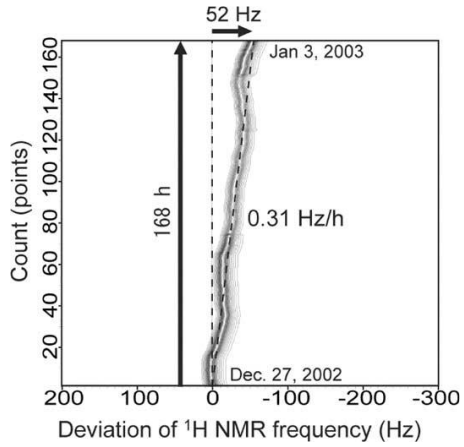

Figure 8. Magnetic field fluctuations for a 21.6 T persistent-mode LTS NMR magnet. Figure adapted from [45] (IEEE, 2004).

40, 30, 20, and 10, then the current is 248, 266, 307, and 468 A, respectively [32]. The *n*-index for the Bi-2223 joint is ~20, whereas that for the REBCO joint is 30–40. Therefore, it may be necessary to take a larger I_c margin for the Bi-2223 joint.

If a soldered lap joint is used in the 30.5 T magnet instead of a superconducting joint, a lap joint length of 100 m would be required to achieve an R_j of 10^{-11} Ω at 4.2 K [46], as shown in Table 1. While the R_j of 0.04 m is a measured value, the other values are estimated using extrapolation. However, it is not feasible to install such a long lap joint (100 m) in the 30.5 T NMR magnet, even if wound around in the form of a coil [34]. Conversely, although a 10-m-long soldered lap joint, corresponding to an R_j of ~10^{-10} Ω, could be installed in the magnet, the number of joints should be reduced to less than 30. This indicates that the superconducting joint is preferred in the ultra-high magnetic field persistent-mode NMR magnet.

High circumferential stress/strain due to electromagnetic force are distinctive features of the ultra-high field LTS/HTS solenoids. Such stress/strain sometimes degrade the REBCO conductor's performance, thereby reducing the I_c and the *n*-index, and increasing the resistance of the circuit. As described before, the maximum permissible resistance for the 30.5 T NMR magnet is 3×10^{-9} Ω, corresponding to a voltage of 6×10^{-7} V if the coil current is ~200 A. This value almost agrees with the voltage criterion per unit length of the HTS conductor for the four-probe I_c measurements, i.e., 10^{-6} V cm^{-1}. Therefore, a slight degradation of the REBCO conductor due to the electromagnetic force is sufficient to degrade the temporal magnetic field stability. The recently performed investigations have demonstrated that the interaction between the axial magnetic field and the screening current tilts the REBCO conductor, resulting in the REBCO conductor degradation [47]. Such phenomena must be considered to suppress the degradation in the field stability.

Table 1. Dependence of R_j on the solder lap length [46].

Lap length (m)	R_j at 4.2 K (Ω)
0.04	2×10^{-8}
1	~10^{-9}
10	~10^{-10}
100	~10^{-11}

2.3.3 Temporal magnetic field drift achieved in the persistent-mode 9.39 T LTS/REBCO NMR magnet with REBCO superconducting joints. As a partial demonstration for the development of the persistent-mode 30.5 T LTS/HTS NMR magnet (1.3 GHz for ^{1}H NMR), a Japanese group developed and operated a persistent-mode 9.39 T (400 MHz) LTS/REBCO NMR magnet with a REBCO inner coil with superconducting joints between REBCO conductors [31]. The REBCO inner coil and LTS outer coil were shunted using individual persistent current switches (PCS) and were operated in each persistent current circuit at 4.2 K.

The magnet was operated in the persistent-mode for approximately two years, and the magnetic field drift was measured as shown in Figure 9. The magnetic field was proportional to the logarithmic time because of the relaxation of the screening current-induced magnetic field. After approximately two years of starting the operation, the drift rate of the magnetic field decreased to ~0.03 ppb/h, which is ten-fold lower than that of the persistent-mode LTS NMR magnet shown in Figure 8. Based on the magnetic field drift rate, the joint resistance is inferred to be < 10^{-14} Ω in an external field of 0.2–0.6 T.

The amplitude of the daily variation in the magnetic field was ±10 ppb, which is twenty-fold smaller than that of the power supply driven mode LTS/HTS NMR magnet shown in Figure 2. However, the mechanism of fluctuation in the persistent-mode is unclear. This could be attributed to the fact that daily room-temperature changes made slight displacements between the superconducting coils and NMR sample at room temperature, resulting in fluctuations in the magnetic field of the NMR sample.

After the magnetic field inhomogeneity was compensated using superconducting and room-temperature shim coils, the NMR spectra of protein samples were obtained successfully under the field-frequency lock operation. Through these experiments, it was demonstrated that the REBCO superconducting joint functions efficiently in a persistent-mode magnet.

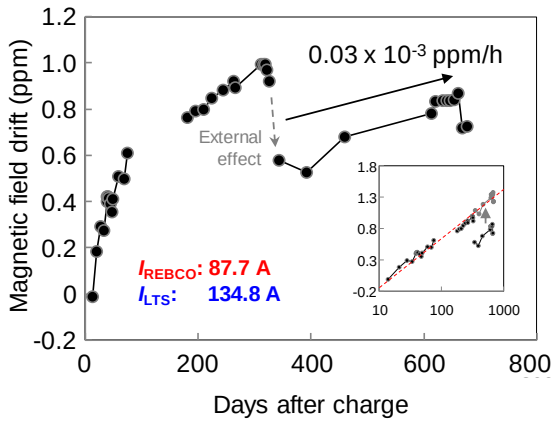

Figure 9. Magnetic field drift of a persistent-mode 9.39 T LTS/REBCO NMR magnet for approximately two years. Figure adapted from [31] (IOP Publishing, 2021).

3. Recent development of the superconducting joint between HTS conductors

The superconducting joint technology is crucial for magnets operated in the persistent-mode, as these magnets can generate a temporally stable magnetic field suitable for NMR and MRI. As aforedescribed, remarkable improvements have been achieved in the superconducting joints between HTS conductors in the last decade. These are summarized in this section as follows:

1. Section 3.1 presents the intrinsic difficulty, history, and recent trends of superconducting joint technology.
2. Sections 3.2, 3.3, and 3.4 present the superconducting joint technology for the REBCO, Bi-2223, and Bi-2212 conductors, respectively, along with their joining processes and superconducting properties.
3. Section 3.5 describes the joint between LTS and HTS conductors, including the potential of forming the superconducting joint.
4. Section 3.6 presents the summary, future prospects and issues to be addressed.

3.1 Overview of the superconducting joint technology for HTS conductors: Intrinsic difficulty, history, and recent trends

The cold-pressed method is used to form superconducting joints between NbTi wires; however, it would be difficult to apply this method in ceramic HTS materials. Another approach to achieving superconducting joint between LTS wires is by a using superconducting solder such as Bi–Pb and Pb–Sn. Details of the soldering joint for LTS conductors are reviewed in [3]. However, the superconducting joint between HTS conductors showing an ultra-low R_j of $< 10^{-11}$ Ω through soldering has not yet been achieved. This can be attributed to the chemical difficulty in forming superconducting joints between ceramic HTS and metallic superconducting solders. Banno et al. [48] recently reported the challenges faced when developing superconducting joints for REBCO using a solder owing to the highly corrosive nature of the REBCO superconducting layer under Sn in the solder.

For the fabrication of the superconducting joint, the HTS conductors should be connected using HTS materials. However, developing this connection based on intuition is a significant challenge because ceramic HTS materials have weak-link characteristics due to their ultra-short coherence length, *d*-wave symmetry of superconductivity, and large electromagnetic anisotropy. Almost all the HTS community researchers had thought it was impossible to develop a superconducting joint that can exhibit a high I_c and an ultra-low R_j between the HTS conductors, and thus, the HTS superconducting joint technology was not earnestly studied for a long time. Conversely, practical HTS conductors with a high J_c and a sufficiently long length, each comprising a superconducting layer with a relatively homogeneous microstructure suitable for developing superconducting joints, were developed in the late 2000s. The development of the HTS magnet technology progressed between the 2000s–2010s, as described in section 2. The HTS superconducting joint technology for developing persistent-mode magnets was long expected in the field of applied HTS.

In 2013, Lee et al. [25] and Park et al. [26][27][28] reported a superconducting joint between REBCO conductors, which had a significant impact on the magnet technology research and materials science. While the magnet technology researchers expected to develop the persistent-mode magnets, the materials scientists expected to create an improved HTS superconducting joint methodology. Lee et al. and Park et al. proposed a direct-type joining method, which had several drawbacks such as weakness against mechanical stresses and an extremely long fabrication time, as described in section 3.2.3. After conducting intensive research in the following years, several groups developed indirect-type joining methods by introducing an intermediate superconducting layer between HTS conductors. As a result, I_c of the joint (I_{cj}) of several hundred amperes and an ultra-low R_j (joint resistance) $< 10^{-11}$ Ω were successfully achieved. Furthermore, a 9.39 T persistent-mode LTS/REBCO NMR magnet was developed using the REBCO superconducting joints. The HTS superconducting joint technology was presented and discussed in the "Joints" sessions during the International Conference on Magnet Technology in 2017–2019 (MT25 [49] and MT26 [50]) and Applied Superconductivity Conference in 2018–2020 (ASC2018 [51] and ASC2020). Therefore, the superconducting joint technology for producing joints between HTS conductors, which was believed to be impossible ten years ago, is a critical research issue today.

Given the recent trends in the progress of HTS superconducting joint technology, Kobayashi et al. developed a superconducting joint resistance evaluation system [52]. Generally, the current decay method [53] is used to evaluate ultra-low R_j. The system efficiently performs the current decay measurement at 4–90 K. Although the closed-loop sample size is fixed, R_j of 10^{-14}–10^{-8} Ω at ~10^3–10^5 s can be easily evaluated. Thus, the development of such evaluation systems accelerates the development of an efficient HTS superconducting joint technology.

3.2 REBCO superconducting joint

3.2.1 REBCO coated conductor (CC). Research and development on REBCO ($REBa_2Cu_3O_y$) are progressing at an accelerated rate because of its advantageous properties such as a high $T_c \approx 90$ K with an optimal oxygen content of $y \approx 6.9$. The nonstoichiometric oxygen content, y, significantly influences the superconducting properties of REBCO. For example, YBCO with $y < 6.3$ does not exhibit superconductivity [54]. Therefore, proper control of y is imperative for a REBCO conductor. Annealing is often performed at ~300–500 °C under sufficiently high oxygen partial pressures (P_{O2}), such as annealing in flowing oxygen gas (oxygen annealing), to achieve a high J_c.

The formation of a biaxially aligned microstructure is essential for fabricating high-J_c HTS conductors [55]. The J_c of REBCO can be enhanced significantly via grain alignment. A general REBCO conductor has a several-micrometers-thick REBCO thin film. The texture of the REBCO thin film strongly depends on the base such as the buffer layer and the substrate. Two types of substrates, the textured buffer type and the textured metal type, are mainly used. The textured buffer type, also called the IBAD substrate, contains textured buffer layers such as MgO or $Gd_2Zr_2O_7$ grown on an untextured substrate with the assistance of an ion beam at a specific angle to obtain a highly biaxially oriented buffer layer [55]. Iijima et al. invented the IBAD substrate in 1991, and since then, it has been researched worldwide and has become one of the most popular substrate choices.

Conversely, the textured metal type, also called the rolling-assisted biaxially textured substrate (RABiTS), can be fabricated using only simple cold rolling and subsequent heat treatment processes at a relatively low cost. RABiTS substrates containing a rare metal Ni–W and a clad-type textured metal substrate that uses inexpensive Cu as a textured layer and reinforced with stainless steel (SUS) have been developed [56][57].

Both the substrate types feature a biaxially aligned buffer layer surface with good lattice matching to REBCO. The several-micrometers-thick REBCO thin film, usually capped with a protective Ag layer, is epitaxially grown from the surface, and the conductor is often electroplated with Cu [15][58].

A < 0.3-mm-thick REBCO conductor as such is also called a coated conductor (CC). The REBCO CC is industrially fabricated by more than ten manufacturers globally. Owing to the REBCO layer's biaxial alignment, CC shows the highest J_c among the superconducting wires even at ultra-high magnetic fields [15][16], thereby promoting active research on REBCO. Owing to the high J_c, CC is used to develop ultra-high field magnets. Previously, a REBCO insert coil was used to generate a field of 45.5 T inside a 31.1 T resistive background magnet [59]. Ultra-high field all-superconducting (LTS/HTS) magnets generating beyond 30 T usually use an inner coil made with the REBCO CC [17][18][19].

3.2.2 Outline of the joining method for REBCO CCs. Industrially fabricated CCs have flat and biaxially aligned REBCO thin films. The epitaxial growth technique is usually used to achieve the REBCO superconducting joint. The REBCO surface is first exposed by removing the metallic layers (Cu and Ag) from a pair of CCs. Then, the epitaxial growth reaction between the REBCO surfaces of the two CCs is promoted. The different joining methods primarily differ in their epitaxial growth processes. Both the direct and indirect methods have been proposed, wherein an additional intermediate material such as a thin film or a bulk is used in the indirect method.

For epitaxial growth, heat treatment is usually performed at temperatures above 800 °C, which often causes oxygen deficiency in REBCO. Thus, sufficient oxygen annealing is required to achieve a high I_{cj} after the epitaxial growth.

In some CCs, the REBCO layer surface is covered with non-superconductive precipitates, rendering it unsuitable for developing the superconducting joint. Therefore, these precipitates should be eliminated to connect the REBCO surfaces.

3.2.3 World's first "superconducting joint" for REBCO CCs. In 2013, Lee et al. [25] and Park et al. [26][27][28] reported that they had successfully developed the world's first "superconducting joint" between REBCO CCs using SuperPower CCs based on an IBAD substrate. They also succeeded in achieving a persistent-mode operation for a small test coil with the superconducting joint. The joining procedure used is as follows:

1. The Ag stabilizer of the CCs was eliminated through chemical etching to expose the REBCO layer.
2. A pair of REBCO layers were directly joined through atomic diffusion with partial melting by heat treatment at 850 °C for 1 min.

Because oxygen in the REBCO layer diffuses during the heat treatment, which could degrade the superconducting properties, it is necessary to introduce oxygen for recovery,

which is essential for the joining technique. In general, it is challenging to supply oxygen to a joining layer, which is considered as a sealed single crystal-like REBCO layer because of the low oxygen diffusion coefficient and the absence of an oxygen diffusion path. This problem was solved by introducing 20-μm micro-holes through a laser drilling technique. The I_{cj} value identical to that of pristine CC (84 A at 77 K, self-field) was obtained by introducing oxygen at 500 °C for 350 h.

Based on the decay rate at the central field of a closed loop with a diameter of 61 mm and five winding turns with one joint, R_j was estimated to be less than 10^{-17} Ω at 77 K for 240 days. This result was the world's first reported persistent current in a REBCO coil.

3.2.4 Superconducting joint technique for REBCO CCs: the iGS joint [29]. For the practical applications of the superconducting joint for REBCO CCs, the joining process must be shortened. The intermediate Grow Superconducting (iGS) joining technique requires a processing time of one day only. In this technique, the REBCO layer is thickened through metal organic deposition (MOD). The joining process is almost similar to the REBCO film deposition process, with a processing temperature of 800 °C and an annealing time of 6 h. Although we first believed that the structure of our REBCO CCs would work effectively to shorten the processing time, in essence, because our joining technique does not depend on the substrate, it can also be applied to IBAD-based CCs. The joining technique is described below.

We used CCs manufactured by Sumitomo Electric Industries. A fine clad tape (Ni/Cu (biaxially oriented layer)/SUS) was used as the substrate. The texture of the REBCO layer depends on the texture of the metal grains of the biaxially oriented Cu layer via buffer layers (CeO_2 / YSZ / Y_2O_3). The REBCO layer has metal grain boundaries of ~100 μm, which act as oxygen diffusion paths. Therefore, we initially thought that it might shorten the processing time. The CCs comprises REBCO / CeO_2 / YSZ / Y_2O_3 / Ni / Cu / SUS. As a REBCO layer, $GdBa_2Cu_3O_y$ (GdBCO) was deposited through pulsed laser deposition (PLD). The oxygen introduction treatment for the GdBCO layer was performed when the furnace cooled from 500 to 200 °C over a duration of 6 h in P_{O2} of 1 atm. The I_c at 77 K in self-field, and conductor width were 160 A and 4 mm, respectively.

The iGS joining technique that applied the thick film technology with MOD is described as follows: When depositing thick films by the MOD, the discharge of CO_2 gas during the pyrolysis process is a concern. To solve this, we developed a process of forming an intermediate layer composed of microcrystalline REBCO and epitaxially growing the same on the CCs. For the standard MOD method, we applied a solution containing the raw materials of REBCO, and a pyrolyzed film was obtained by heat treatment at 500 °C. During the thickening process, a pyrolyzed film was stacked and heat-treated at 800 °C to obtain an epitaxial film of REBCO. The reaction process is given as:

$$(1/2)\mathrm{RE_2O_3} + 2\mathrm{BaCO_3} + 3\mathrm{CuO} \rightarrow \mathrm{REBa_2Cu_3O_{6.5}} + 2\mathrm{CO_2}$$

However, for thick films, the decomposition of $BaCO_3$ and crystallization of REBCO begin from the top surface, and based on the time taken to discharge the internally generated CO_2, the decomposition of $BaCO_3$ is insufficient. As a result, REBCO epitaxial films cannot be obtained in a short time. Therefore, to enhance the decomposition of $BaCO_3$, heat treatment is performed at 800 °C under P_{O2} = 1 atm to form a porous REBCO film in a microcrystalline state. Furthermore, by performing heat treatment at 800 °C under $P_{O2} = 10^{-4}$ atm, which are the crystal growth conditions of REBCO, a thick porous REBCO film was epitaxially grown in a short time. This thick film was similar to the joining as it does not effectively discharge gas. Therefore, we concluded that this thickening technology could be used in a REBCO joining technique.

Figure 10 shows an example of a joint configuration. The Cu stabilization and Ag protective layers of the two CCs were removed to expose the GdBCO layer, and the surfaces of the GdBCO layer and joining strap were arranged face to face. Although the joining strap has the same structure as that of the CCs, it has a microcrystalline REBCO layer on the surface, which is the critical point for the joining technique. This microcrystalline REBCO layer is used as an intermediate layer. We named the resultant joint acquired through this joining technique as an iGS joint owing to the "intermediate layer" that grows and joins the REBCO.

As mentioned before, the iGS joint uses a microcrystalline REBCO as an intermediate layer, which is not epitaxially grown before the heat treatment for joining. The scanning electron microscopy (SEM) images of the microcrystalline layer revealed the crystal grain size to be between 20–200 nm, whereas the ring-shaped 103 (REBCO) pattern in the 2D X-ray diffraction profile indicated a polycrystalline of random orientation.

The specific joining procedure is described below. Two CCs were arranged side by side, with the superconducting surfaces of both CCs and the joining strap facing each other and bolted using a SUS jig. The treatment conditions for joining were the same as that used for the deposition of the GdBCO film, i.e., at 800 °C under $P_{O2} = 10^{-4}$ atm. This low processing temperature reduces the risk of CC deterioration, making it an essential advantage of the iGS joint. During joining, the microcrystalline layer begins to grow on the GdBCO layer, and the GdBCO layers join. Grain growth occurs owing to the movement of grain boundaries, and there is a thermodynamic driving force to reduce the total boundary area. Considering that the crystal growth rate is approximately

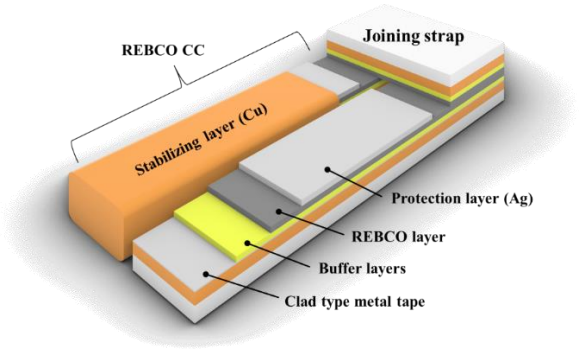

Figure 10. Sumitomo REBCO CC architecture and an example of a joint configuration.

40 nm/min, a joining layer of 200 nm was completed within 20 min. After the superconducting joining process, oxygen introduction treatment was required as in average REBCO production. Oxygen was introduced for approximately 6 h as the furnace cooled from 500 °C to 200 °C in P_{O2} = 1 atm. The entire joining process took approximately 24 h, which we believe is practically short for magnet manufacturing.

Figure 11 shows the cross-sectional high-angle annular dark-field scanning transmission electron microscopy (HAADF-STEM) images of a joint sample heat-treated at 800 °C for 20 min [60]. We used YBCO instead of GdBCO as the intermediate layer material to identify the interface between the intermediate layer and the CC. Figures 11(b) and 11(c) show the high-resolution image of each interface of (Y,Gd)BCO/GdBCO indicated by the black frame (Figure 11(a)). In the HAADF-STEM image, differences in the atomic weight appear as light and dark, and Y, an element lighter than Gd, appears dark. An arrow seen in Figures 11(b) and 11(c) show the interfaces estimated from the contrast, and each interface is joined at the atomic level. These results revealed that the microcrystalline REBCO layer grows epitaxially from the interface of each REBCO layer, and finally, the three REBCO layers join at the atomic level, making it ideal as the superconducting joint.

A four-terminal method using an electric field criterion of 1 μV was applied to measure the current–voltage (*I*–*V*) characteristics in liquid N_2 (77 K) under the self-field. The I_{cj} was 71–110 A whereas I_c of the virgin CC was 160 A. A small pancake coil with a self-inductance of 53.5 μH was prepared. The R_j at 77 K in self-field was evaluated based on the temporal magnetic field decay, and R_j of ~5 × 10^{-13} Ω was demonstrated, as shown in Figure 12. The decrease in the corresponding R_j with time can be attributed to the relaxation of the screening current. Furthermore, in a recent study, it has been confirmed that the comparable superconducting characteristics for the iGS joint can be achieved on IBAD-based CCs.

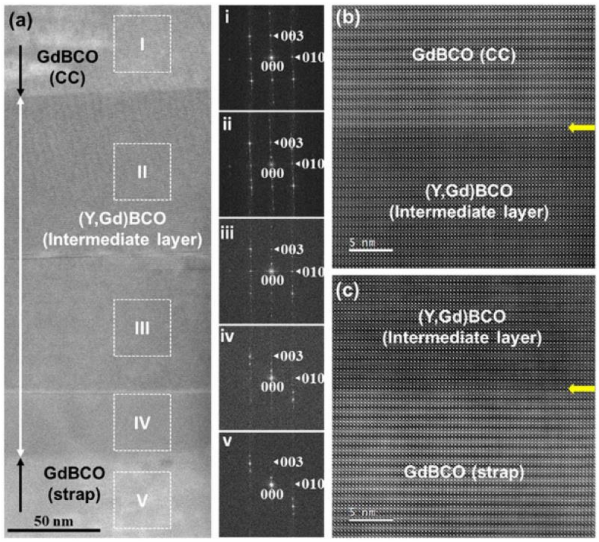

Figure 11. (a) Cross-sectional HAADF-STEM image of a joint sample. (b) and (c) High-resolution HAADF-STEM images of the boundaries. Figure adapted from [60] (IOP publishing, 2020).

The transport I_{cj}–*B*–*T* characteristics were evaluated under the criterion of 1 μV, as shown in Figure 13 [31]. A joint sample showed a self-filed I_{cj} of 70 A at 77 K. At 4.2 K, high in-field I_{cj} of 740 and 405 A at 1 and 10 T (parallel to the tape plane), respectively, were achieved in this sample. The *n*-value for the power-*n* model [3] increased with a decrease in the temperature or field, and an *n*-value of 30–50 was confirmed at 4.2 K. Such I_{cj}–*B* characteristics can be suitable for operating in the persistent-mode at 4.2 K. Furthermore, the in-field I_c at 50 K was ~200 and ~100 A at 1 and 5 T, respectively, which indicates that the iGS joint can also be applied to persistent-mode magnets operated at relatively higher temperatures.

The iGS joint was used for the REBCO inner coil of the 9.39 T LTS/REBCO NMR magnet (400 MHz for ^{1}H NMR) [31], which was operated in the persistent-mode at 4.2 K to achieve a stable magnetic field, as described previously in section 2.3.3. An ultra-low R_j, lower than 10^{-14} Ω at 0.2–0.6 T, was estimated during the continuous operation approximately two years. This result clearly demonstrates that the iGS joint can be applied to a persistent-mode magnet.

3.2.5 Joining method by Furukawa Electric Co., Ltd. In 2016, Furukawa Electric Co., Ltd. held a press release [61] pertaining to the superconducting joint technology for the REBCO CCs. A few years later, the indirect-type joining method [62], ultra-low in-field R_j values of a coil [63] or a single-turn loop [64], and I_{cj}–*B*–*T* characteristics [65] were reported. In these reported studies, the commercially available REBCO CCs, manufactured by SuperPower Inc., were used.

The joining method is elucidated below [62]:

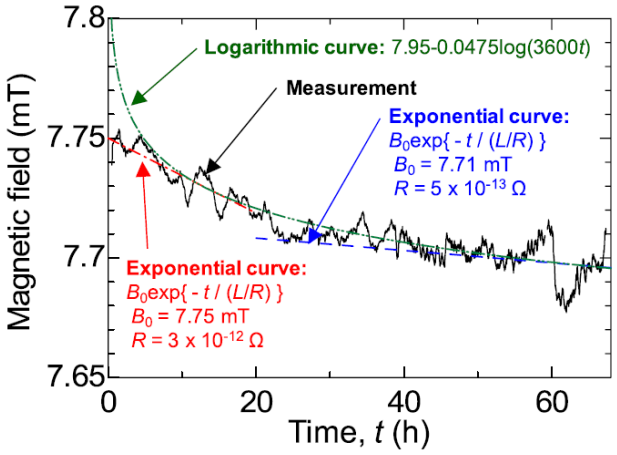

Figure 12. Decay curve of the central magnetic field during the persistent-mode operation in liquid N_2 (77 K) and self-field. The solid line shows averaged data of the measured magnetic field. Calculated decay curves corresponding to $R = 3 \times 10^{-12}$ Ω and 5×10^{-13} Ω are also shown for comparison. Figure adapted from [29] (IOP publishing, 2017).

1. The liquid solution comprising REBCO is applied to the exposed REBCO surface of the two CCs.
2. After pre-calcination at ~500 °C, the two CCs are overlapped and brought in contact to connect the intermediate layer.
3. The connected part is compressed using a mechanical pressure and heat-treated at ~800 °C to promote epitaxial growth.
4. Oxygen annealing is performed.

The indirect-type superconducting joint was developed as the iGS joint. A thin film was formed between the REBCO layers of a pair of CCs as an intermediate layer. However, the processing time was not revealed.

Current decay measurements were performed for a single-turn loop with self-inductance of 0.105 μH. Ultra-low R_j of less than 10^{-13} Ω was observed at ~35–50 K and 0–3 T [64]. A larger coil with self-inductance of 1.5 mH also yielded an ultra-low R_j of ~10^{-12} Ω in the field decay measurements at 20 K in self-field [65]. At 1 T, the decay corresponded to a relatively higher resistance of ~10^{-11}–10^{-10} Ω in the coil, which can be attributed to the screening current-induced magnetic field, as discussed in section 2.

The transport I_c–B–T characteristics of the joint are reported in [65], which are suitable for application requiring persistent-mode magnets. A joint sample showing a self-field I_{cj} of ~100 A at 77 K under 1 μV criterion was used. The in-field I_{cj} at 4 K was ~700 and ~400 A at 0.1 and 1 T, respectively. Furthermore, I_{cj} at 0.1 T was ~600, ~350, and ~60 A at 20, 50, and 77 K, respectively. Moreover, sufficiently high n-value

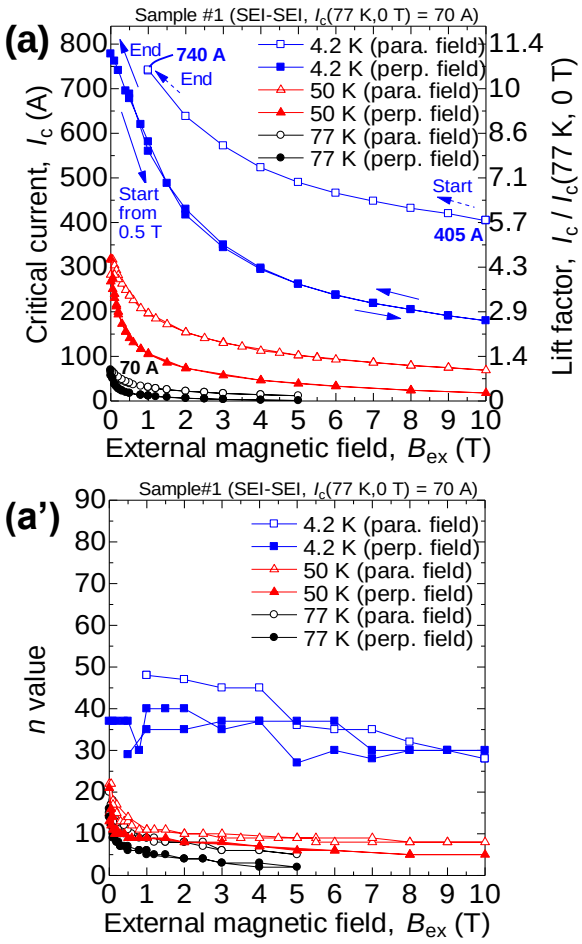

Figure 13. Transport I_c–B–T characteristics including n-values under a 1 μV criterion of an iGS joint sample. Figure adapted from [31] (IOP publishing, 2021).

was observed. The anisotropy, hysteresis behavior of I_{cj}, and pinning mechanism were also discussed.

Based on the superconducting properties, it can be ascertained that the superconducting joint technology developed by Furukawa Electric Co., Ltd. is applicable to persistent-mode NMR and MRI magnets. Their primary aim is to develop a REBCO MRI magnet, which can operate at temperatures as high as 50 K [62], using this superconducting joint technology.

However, the formation mechanism of this superconducting joint is still unclear as no microstructural observation results of the joint part, especially at the interface, were found.

3.2.6 Other joining methods. Jin et al. [66] proposed a CJMB (crystalline joint by melted bulk) method that uses a REBCO bulk as an intermediate layer. The REBCO thin film of the CC acts as a seed crystal in the melt-solidified REBCO bulk. The YBCO or YbBCO bulk layer were selected to connect the GdBCO CCs because of the peritectic temperature

of GdBCO, which is higher than that of YBCO and YbBCO by ~50 and ~100 °C [67], respectively. The superconducting joint was formed using a ~0.1-mm-thick polycrystalline YbBCO sheet by heat treatment above 900 °C [68][69]. A current decay measurement was performed at 77 K in self-field for a closed-loop coil with self-inductance of 0.12 mH. As a result, an R_j of ~8×10^{-13} Ω was successfully achieved [68]. Conversely, typical self-field I_{cj} at 77 K is as low as ~10 A. This could be because of the fact that heat treatment at high temperatures can degrade the I_c of the CC. Microstructural observation revealed that the epitaxial growth occurred only in a small part of the joint interface [69], which resulted in low I_{cj}.

Teranishi et al. [70][71][72][73] developed another joining method. Similar to the joining method described in section 3.2.5, an additional precursor film was formed on the exposed REBCO surface of the CC using both MOD and PLD methods. An apparatus was developed with a heater and loading equipment for joining. After two CCs with the precursor film were placed face to face, crystallization was performed of the joint part in the apparatus by heat treatment under low P_{O2} with uniaxial pressure. The joining mechanism was considered based on the relationship between the effective joint area and uniaxial pressure during heat treatment. Unfortunately, the joint samples yielded low I_{cj} of several amperes at 65–77 K. They did not perform current decay measurement. The ultra-low R_j by the superconducting joint was not demonstrated.

3.2.7 Summary and future prospects of REBCO. The recent successful development of the HTS superconducting joint technology has started from the superconducting joint between the REBCO CCs. Furthermore, the development of the iGS joint has significantly progressed. High I_{cj} and ultra-low R_j applicable for persistent-mode magnets have been demonstrated. The iGS joints were successfully implemented in an LTS/REBCO NMR magnet operated in the persistent-mode, which generated the temporally stable magnetic field.

The I_c of the iGS joint, determined by the J_c (//*c*) for REBCO and the joint area [29], was lower than that of the virgin CC. The I_{cj} comparable to I_c of the tape can be achieved based on the extensive joint area.

The technology used to form clean REBCO surfaces, including the elimination of non-superconductive precipitates for the REBCO surface and the optimization of the metallic-layer removal methods, should be discussed further. These processes should not damage the REBCO CCs. Furthermore, the fabrication condition of the REBCO CC might need to be reconsidered to eliminate the precipitates.

In the future, the iGS joint will be installed to the persistent-mode 30.5 T LTS/HTS NMR magnet (1.3 GHz for ^{1}H NMR) shortly. The high-performance REBCO superconducting joint enables ultra-high field or He-free persistent-mode magnets, which will be used for applications in NMR and MRI in the future.

3.3 Bi-2223 superconducting joint

3.3.1 Bi-2223 tape. Bi-2223 [$(Bi,Pb)_2Sr_2Ca_2Cu_3O_y$] shows a higher T_c of ~110 K compared to REBCO. High-I_c polycrystalline Bi-2223 conductors can be fabricated through the powder-in-tube (PIT) method using Ag (or Ag alloy) tubes similar to the LTS conductors. The tape-shaped (~4-mm-wide and ~0.3-mm-thick) multifilamentary Bi-2223/Ag conductors, attributed to the flat rolling process, which is crucial for fabricating conductors with the strongly *c*-axis grain-aligned microstructure, have historically been developed [74].

Ag sheathed multifilamentary Bi-2223 tapes are commercially available. Sumitomo Electric Industries mass-produces DI-BSCCO®, the long-length Bi-2223/Ag tapes with 121 filaments [74][75][76]. DI-BSCCO tape shows high I_c characteristics and is used to develop high-field magnets. For example, the 24 T driven mode LTS/HTS NMR magnet (1.02 GHz for ^{1}H NMR) comprised the Bi-2223 most-inner coil made using DI-BSCCO [22][77]. A 25 T cryogen-free research magnet was also developed using DI-BSCCO [78].

3.3.2 History of the development of superconducting joint between Bi-2223 tapes. Fabrication of the superconducting joint between the Bi-2223/Ag tapes was first attempted by Tkaczyk et al. in 1993 [79]. The two exposed cores of the monofilament tape were directly connected in the lap joint configuration. The Bi-2223/Ag tape core could be exposed by peeling off or chemically etching the Ag sheath from one side of the tape [3]. The superconducting joint was achieved after high-pressure pressing and heat treatment. The corresponding I_{cj} was lower than the I_c of the tape. Furthermore, in the reported studies mentioned in [3], it was shown that the Bi-2223 superconducting joint can be formed in monofilament Bi-2223/Ag tapes and Bi-2223 polycrystalline bulks. Similar to the study by Tkaczyk et al. [79], in these studies also, the direct method was employed through high-pressure pressing above several hundreds or thousands of MPa and heat treatment.

However, the superconducting joint technology for multifilamentary Bi-2223/Ag tapes exhibit several limitations. Owing to the shape of the tape, exposing most Bi-2223 filaments to connect with a sufficient area is tricky. The filaments only on the surface region of the tape can be exposed by removing the Ag sheath, as in the case of the core of the monofilament Bi-2223/Ag tape. Forming a superconducting joint by connecting these surface filaments was attempted. In the early 2000s, the indirect method was proposed using the intermediate Bi-2223 material to connect as many filaments as possible. Kim et al. [80] used the monofilament tape as the intermediate material. Wang et al. [81] sandwiched the Bi-

2223 precursor powder between the exposed filaments of two tapes. A new polycrystalline Bi-2223 layer was synthesized between the tapes by heat treatment, thereby achieving the superconducting joint. When the Bi-2223 intermediate layer was synthesized, grain coupling was formed at the joint interface. However, a high I_{cj} was not observed in these studies, partly because in the early 2000s, the I_c of the then available tapes was not high.

In 2009–2010, Guo et al. [82][83] demonstrated superconducting joints between commercially available 4.3-mm-wide and 0.22-mm-thick tapes Bi-2223/Ag tapes with 61 filaments developed by Beijing Innova Superconductor Technology Co., Ltd. The Ag sheath of the tapes was chemically etched using NH_3/H_2O_2 (aq). The exposed filaments were directly faced or indirectly overlapped by sandwiching Bi-2223 precursor powder as specified in [81]. To connect the filaments, heat treatment was performed at 800 °C for 2 h with uniaxial pressure of 3 MPa. The joint samples yielded a self-field I_{cj} of several tens of amps at 77 K. Therefore, the Bi-2223 superconducting joint was successfully achieved between the commercially available Bi-2223/Ag multifilamentary tapes. Compared to the direct method, the indirect method showed relatively better reproducibility. Furthermore, it was revealed that pressing at a high pressure before heat treatment is not always needed to form a superconducting joint. Such a process can deform the tape, resulting in an excessive decrease in I_c.

This indirect method was applied to DI-BSCCO®, the practical Bi-2223/Ag tape. Ebara et al. [84][85] fabricated a loop sample having one Bi-2223 superconducting joint, with the surface filaments of both ends were exposed by etching the Ag sheath with a knife. After sandwiching precursor powder between the exposed filaments to form a closed-loop shape, heat treatment was performed at 838 °C for 100 h under uniaxial pressure. An R_j of ~10^{-13} Ω at 77 K was evaluated by an original method using current decay. Furthermore, microstructural observation revealed that the polycrystalline intermediate layer was well connected to the Bi-2223 filaments. Conversely, I_{cj} was low even in self-field. With applied current of ~2 and ~10 A at 77 and 4 K, respectively, the joint generated a voltage of 1 μV.

There were two issues that could suppress I_{cj} of the Bi-2223 superconducting joint between the DI-BSCCO tapes. One is the number of the connected filaments. The number was only ten percent of that of the total filaments in the joint for DI-BSCCO. I_{cj} can be improved by increasing the number of filaments connected with a sufficient area for a large current path. Second is the J_c properties of the Bi-2223 intermediate layer. A Bi-2223 sintered bulk is used for the current lead of superconducting magnets [86]. The typical bulk exhibits J_c lower than 1 kA cm^{-2} at 77 K, which is two orders of magnitude lower than that of the tape. If a Bi-2223 intermediate layer in the superconducting joint shows significantly low J_c, a high I_{cj} cannot be achieved even if most filaments are successfully connected. Thus, it is essential to synthesize a Bi-2223 intermediate layer with sufficiently high J_c to improve I_{cj}. Based on this strategy, Takeda et al. successfully demonstrated the Bi-2223 superconducting joint exhibiting high I_{cj} between DI-BSCCO tapes [30]. Details of this superconducting joint technology are described in section 3.3.3.

Jin (Kanazawa) et al. proposed the "joint by incongruent melting (JIM) method," which is an entirely different concept used to form the Bi-2223 superconducting joint between DI-BSCCO tapes [87]. The superconducting joint can be formed through the incongruent melting between Bi-2223 tapes (Bi-2223 is known to melt incongruently at high temperatures [88][89]). Details of this superconducting joint technology are described later in section 3.3.4.

3.3.3 High I_{cj} Bi-2223 superconducting joint [30] A Japanese group, which included one of the authors of this paper, developed the polycrystalline Bi-2223 materials that exhibit high J_c [90][91][92][93]. Based on these studies, they established the strategy for achieving a high J_c in the materials. Takeda et al. used the strategy and the slurry process to fabricate the polycrystalline thick film material exhibiting high J_c [94]. A high J_c of ~8 kA cm^{-2} at 77 K was achieved, which was approximately one order of magnitude higher than that of the typical Bi-2223 bulk [86]. Thus, the slurry process seemed suitable to form an intermediate layer of the indirect-type superconducting joint between the practical Bi-2223 tapes, DI-BSCCO®. We used the slurry process to develop a straight lap joint sample. The Ag sheath of two short tapes was mechanically removed by peeling to expose the surface filaments. Then, a precursor film of an intermediate layer was formed between the exposed filaments of the two tapes through the slurry process. After uniaxial pressing at ~200 MPa, heat treatment was performed at 810 °C under P_{O2} = 3 kPa, which was suitable for fabricating a thick film exhibiting a high J_c. The sample yielded an I_{cj} of ~10 A at 77 K in self-field. Therefore, we confirmed that forming an intermediate layer through the slurry process was effective for the superconducting joint between the Bi-2223 tapes.

However, the other severe issue pertaining to the number of connected filaments persists. To expose a larger number of the filaments, we attempted to apply the mechanical polishing technique with an angle of < 1° against a tape. Although this technique is practically used to prepare samples for microstructural observations, the polishing angle is usually > 5°. Therefore, it was challenging to polish the tape with an angle of < 1°. We optimized the polishing conditions, including adjusting the jig to fix the polishing angle. As shown in Figure 14, we were able to obtain the surface where almost all filaments were exposed by polishing the tape after peeling off the Ag sheath. Furthermore, microstructural observations

for the surface revealed minimal damage to the Bi-2223 crystals of each filament, indicating that the surface is applicable to form the superconducting joint. We used the polished tapes to fabricate the joint samples as shown in Figure 15. The slurry process, uniaxial pressing, and heat treatment processes were applied. Transport measurement at 77 K was performed by immersing the joint samples in liquid N_2, which confirmed the formation of the superconducting joint. I_{cj} was improved with an increase in the number of exposed and connected filaments, as shown in Figure 16. For a sample with almost all filaments connected, a self-field I_{cj} of 61.4 A was acquired under a 10^{-9} Ω criterion (Joint C in Figure 16). Furthermore, the transport measurement for this sample in liquid He revealed a self-field I_{cj} of over 400 A at 4.2 K. Therefore, we successfully demonstrated the superconducting joint between the Bi-2223 tapes exhibiting high I_{cj}.

An in-field I_{cj} of several hundred amps under a 10^{-9} Ω criterion was observed at 4.2 K in our recent studies [95]. A closed-loop sample exhibited ultra-low R_j characteristics, typically less than 10^{-12} Ω [96]. However, in the studies described above, we used the DI-BSCCO "Type H" tape, which is not practically applicable to ultra-high field magnets because of its insufficient mechanical strength [74][97]. The high-strength DI-BSCCO "Type HT" tapes, which are Type H tapes laminated with reinforcement materials, are usually used for high-field magnets. We also developed a joining method for the high-strength tapes, including the removal of the reinforcement materials [98]. Based on this method, we have developed a persistent-mode 9.39 T LTS/Bi-2223 NMR magnet (400 MHz for ^{1}H NMR). This joining method was applied to a Bi-2223 insert coil wound with one high-strength Type HT tape. In the stand-alone test, the insert coil successfully operated at 4.2 K in the persistent-mode with an R_j of ~10^{-12} Ω. We plan to develop a persistent-mode LTS/Bi-2223 NMR magnet using this insert coil. Furthermore, we have planned to generate a stable field, similar to the LTS/REBCO NMR magnet shown in section 2.3.3. Details of these studies will be reported elsewhere.

3.3.4 Bi-2223 superconducting joint through the incongruent melting process. Jin (Kanazawa) et al. proposed a simple joining method called the JIM method for DI-BSCCO® tapes, which uses the incongruent melting of Bi-2223 [87]. The process is as follows: Two Bi-2223 tapes are ground using sandpaper and the surface filaments are exposed. After two tapes are placed together, they are heat-treated at 890 °C for 1 min in a spot heating furnace. The joint interface is formed by the incongruent melting of Bi-2223, resulting in a superconducting joint. The complex constituent phases, such as Bi-2223, (Bi,Pb)-2212 [$(Bi,Pb)_2Sr_2CaCu_2O_y$], (Bi,Pb)-2201 [$(Bi,Pb)_2Sr_2CuO_y$], Ca-Cu-O, Ag, and others, were confirmed at the joint part, which includes the joint interface and the tapes [87][99]. The main phase of the joint interface was probably (Bi,Pb)-2212. The Bi-2223 phase remains at the interface because of the T_c of ~107 K of the joint part, as evaluated by transport I_{cj}–T measurements. Although oxygen annealing was performed at 350 °C for 10 h under P_{O2} of 1 atm after joining, it may not be necessary for controlling the superconducting properties.

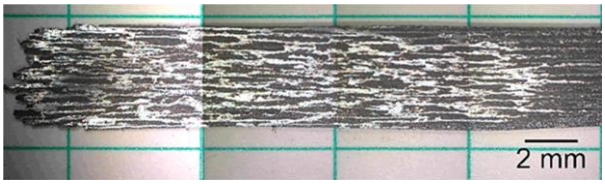

Figure 14. Photograph of a DI-BSCCO tape after polishing at a low angle to expose a large number of the filaments. Figure adapted from [30] (IOP publishing, 2019).

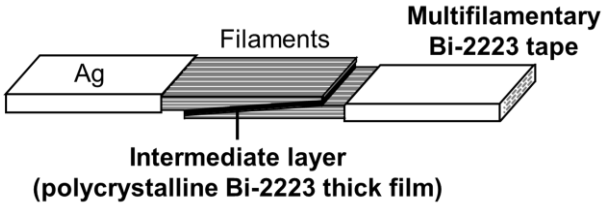

Figure 15. Schematic of configuration of a joint sample showing high I_{cj} between multifilamentary Bi-2223 tapes. A large number of the filaments were exposed by polishing the tape at a low angle against its surface.

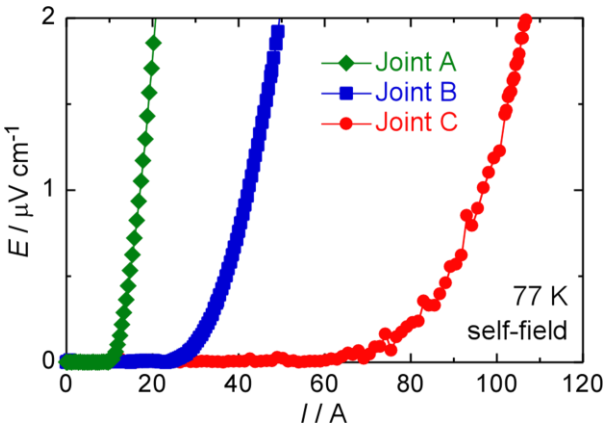

Figure 16. *E–I* curves for joint samples at 77 K, self-field. The number of connected filaments was ~15, ~50, and more than 100 in Joint A, B, and C, respectively. Figure adapted from [30] (IOP publishing, 2019).

Transport I_{cj}–B–T properties were evaluated under 1 μV criterion. A joint sample yielded a self-field I_{cj} of 12 and 177 A at 77 and 4.2 K, respectively, and in-field I_{cj} at 4.2 K, 1 T was ~70 A with an n-index of ~5. A significant increase in I_{cj} with a decrease in temperature can be attributed to the (Bi,Pb)-2212 phase at the joint interface because T_c of the oxygen-annealed (Bi,Pb)-2212 phase is comparable to or less than 77 K [100]. For magnet applications operated in the persistent-mode, I_{cj} characteristics should be improved further. A recent study revealed that a self-field I_{cj} at 77 K can be improved by optimizing the heat treatment condition or joining multiple positions [101].

Furthermore, current decay measurements were performed for a closed loop sample with a superconducting joint [87]. Self-inductance of the sample was 0.10 mH. As a result, self-field R_j of ~10^{-12} and ~10^{-13} Ω was observed at 77 and 4.2 K, respectively.

3.3.5 Summary and future prospects of Bi-2223. High I_{cj} and ultra-low R_j for the Bi-2223 superconducting joint were achieved. The implementation of the joint in an LTS/Bi-2223 NMR magnet is currently in progress. However, several issues pertaining to the application of the joints to the practical persistent-mode ultra-high field magnets need to be addressed.

Our recent study on the joints using the Bi-2223 intermediate layer revealed that it is difficult to reproducibly achieve high I_{cj} between the both ends of coil winding [98]. In the JIM joint, the joint for the small coil was reported [87]. The I_{cj} for the coil was insufficient for a practical magnet operated in the persistent-mode. Therefore, an improved joining method needs to be established applicable for a coil. This could lead to generation of a high magnetic field in the persistent-mode, which in turn could demonstrate that the Bi2223 superconducting joint is applicable to ultra-high field magnets operated in the persistent-mode.

The practical persistent current switch (PCS) is also essential for developing Bi-2223 persistent-mode magnets. In general, a small heater is used for the PCS function to utilize the normal transition of a part of the conductor in a magnet. However, for the PCS of a Bi-2223 magnet, a small heater would be inadequate as a Bi-2223 tape contains a high concentration of Ag [102]. The Bi-2223 tape shows high thermal conductivity and low electrical resistivity in the normal conducting state. Therefore, for Bi-2223 persistent-mode magnets, PCS with sufficient off-resistance should be developed as well as the superconducting joint.

3.4 Bi-2212 superconducting joint

3.4.1 Bi-2212 wire. Bi-2212 [$Bi_2Sr_2CaCu_2O_y$] shows T_c < 95 K, which depends on the nonstoichiometric oxygen content, y. The PIT method using Ag (or Ag alloy) tube is used to fabricate the polycrystalline wires as Bi-2223/Ag tapes. The difference lies in the shape of the conductor as the flat rolling process is not indispensable for the grain alignment of Bi-2212. The melt process is performed to achieve grain alignment [15][16]. As a result, round or rectangular wires showing high I_c characteristics were developed. Generation of a high field of 25.05 T with a 5.11 T Bi-2212 insert magnet within a 19.94 T resistive outer magnet was demonstrated [103].

Superconducting joints between the reacted Bi-2212 wires were studied, which have already been reviewed in [3]. Conversely, the wind-and-react (W&R) method [104] is usually employed to fabricate Bi-2212 magnets [16][105]. Recently, superconducting joint technology using unreacted wires has been developed, wherein the heat treatment performed to form the superconducting joint and prepare the Bi-2212 coils can be conducted simultaneously in the same furnace.

3.4.2 Superconducting joint using Bi-2212 unreacted wires. Chen and Trociewitz et al. [106][107] proposed a joining method using the PIT melt process to fabricate a short joint sample and a coil sample with a joint. Standard PIT Bi-2212/Ag multifilamentary unreacted round wire with a diameter of 1.3 mm, manufactured by Oxford Superconducting Technology, was used. Firstly, the Bi-2212 filaments were exposed by chemical etching using NH_3/H_2O_2 (aq). The two etched wires were placed in the praying-hands configuration, as shown in Figure 17(a). After inserting the two wires into a Ag cup, a joint matrix of 2 wt%-Ag-premixed Bi-2212 powder (manufactured by Nexans SuperConductors) was poured into the Ag cup, as shown in Figure 17(b). A Ag plug was used to compress the powder and seal the open end of the Ag cup. The joint was uniaxially pressed at ~700 MPa, as shown in Figure 17(c), and heat-treated in 1 bar flowing oxygen under the typical Bi-2212 wire fabrication condition.

Transport I_{cj}–B properties at 4.2 K for the short joint sample were evaluated. A high in-field I_{cj}, comparable to the conductor sample, was observed. I_{cj} determined by 0.2 μV criterion was ~900 and ~500 A in self-field and at 10 T, respectively. In contrast, a lower n-value of 8–10 compared to that of Bi-2212 conductor (i.e., 18–20) was reported, which indicates low intergranular connectivity in the Bi-2212 joint part.

A closed loop coil sample with self-inductance of 15.3 μH having a superconducting joint was prepared. A current decay measurement at 4.2 K in self-field was performed, as shown in Figure 18. A slow decay was observed. The corresponding R_j was lower than 5×10^{-12} Ω at 6–7×10^4 s. The decrease in the decay rate with time can be attributed to the relaxation of the screening current, as discussed in section 2. Therefore, the potential for a persistent-mode operation of a Bi-2212 coil was successfully demonstrated.

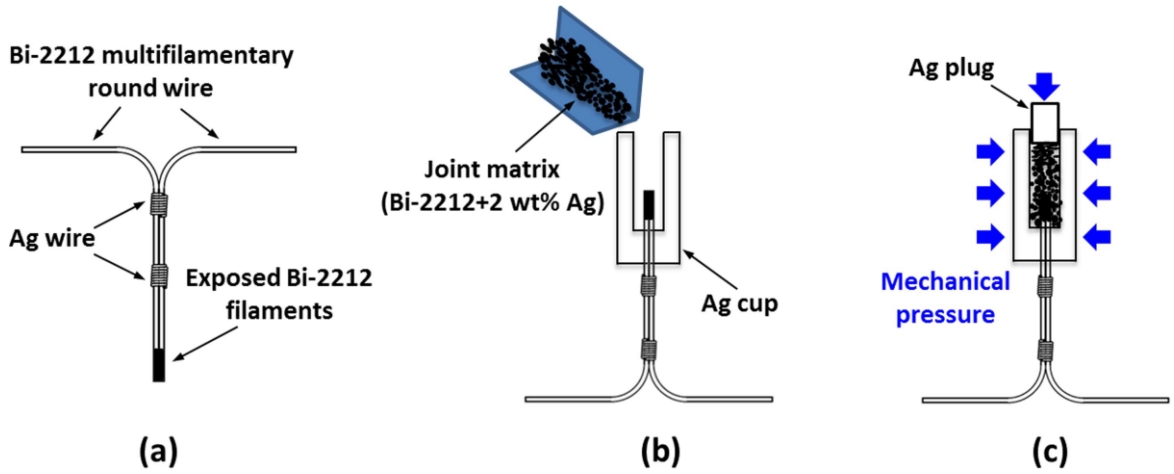

Figure 17. Fabrication method of the superconducting joint between Bi-2212 wires. Figure adapted from [106]. (IOP publishing, 2017).

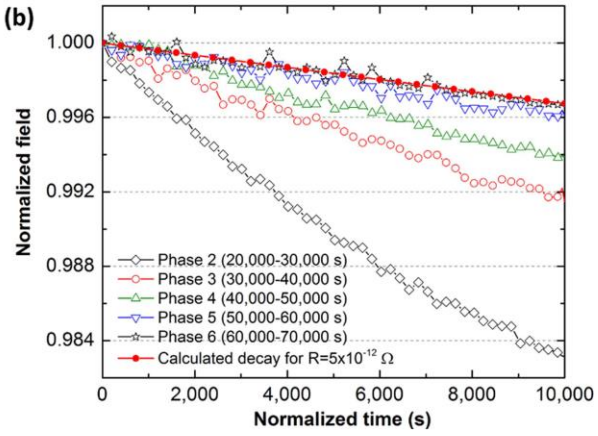

Figure 18. Normalized current decay behavior at 4.2 K of a Bi-2212 coil sample. A calculated decay corresponding to $R = 5 \times 10^{-12}$ Ω is also shown for comparison. Figure adapted from [106]. (IOP publishing, 2017).

Mousavi et al. [108] determined the best joint assembly for the highest I_{cj} through the optimization of this joining method by exploring different joint structures and methods to expose the filaments. To expose the filaments, the chemical etching using NH_3/H_2O_2 (aq) required careful optimization to avoid causing damage to the filaments. Polishing the wires was an efficient approach to expose the filaments without damaging them. Furthermore, large voids were observed in the joint region owing to the volume reduction of the powder during the melt process, which reduced the I_{cj}.

3.4.3 Summary and future prospects of Bi-2212. The Bi-2212 superconducting joint technology, which enables high I_{cj} and ultra-low R_j, has already been established. Given the fact that two different research groups succeeded in developing the superconducting joint exhibiting high I_{cj} by using the same method, the reproducibility seems to be sufficiently high. Conversely, transport I_{cj}–B and self-field R_j were evaluated only at 4.2 K. Therefore, the transport I_{cj}–B–T and R_j–B–T characteristics should be explored as well.

Furthermore, the ultra-low R_j ($< 5 \times 10^{-12}$ Ω) was observed only in a small coil with self-inductance of 15.3 μH. The induced current in the coil (~71 A) was much lower than the I_{cj} (~900 A) of the short joint sample. Therefore, superconducting joint technology for persistent-mode magnets can be improved significantly. Development of practical persistent-mode magnets with superconducting joints including an LTS/Bi-2212 NMR magnet should be attempted. The PCS is also important because of the high concentration of Ag in the Bi-2212 wire.

In terms of materials science, the superconducting joint between the reacted Bi-2212 wires is worth discussing. The JIM method [87] for the superconducting joint between Bi-2223 tapes might also be suitable for joining reacted Bi-2212 wires because the melt process without decomposition of Bi-2212 can be utilized.

3.5 Joint between HTS and LTS conductors

Some studies have reportedly attempted to develop superconducting joints for HTS–HTS or HTS–LTS conductors using the superconducting solder. However, as mentioned in section 3.1, no study has thus far demonstrated an ultra-low R_j less than 10^{-11} Ω. Conversely, resistive (non-superconducting) joining methods such as soldering or ultrasonic welding for HTS conductors have been extensively investigated. These methods could be applied to joints between HTS and LTS conductors showing substantially low resistances if the joint area was extensible. In the following

sections, we review the attempts and difficulties of superconducting joint for HTS conductors by soldering. Furthermore, we describe various joining methods for HTS conductors with substantially low resistance.

3.5.1 Attempts and difficulties of superconducting joint for HTS conductors by soldering. The REBCO thin film of a CC is corrosive under exposure to Sn in the solder, it is difficult to achieve a superconducting joint between a REBCO CC and the solder including Sn [48]. In contrast, Mousavi et al. [109] attempted to form the superconducting joint between reacted Bi-2212/Ag wires through soldering. A two-stage process was developed at 350 °C. First, pure molten Sn was used to remove the Ag matrix, and second, it was immersed in Pb–Bi to replace the Sn. However, a thin layer of Sn–O still remained at the interface between the Bi-2212 filaments and the solder. As a result, the joint had a finite resistance even at low currents.

Matsumoto et al. [110] reported a method for joining a Bi-2223 tape and NbTi wire using a Bi–Pb–Sn solder. The joints were fabricated in the solder by the in-situ sheath-dissolution method at 400 °C, in which the NbTi/Cu wire and Bi-2223/Ag tape were dipped in the melted solder. The *V–I* and *R–T* curves suggested the formation of a superconducting joint or a resistive joint with a very low resistance (less than several nΩ). However, the thin layer containing Sn at the interface between the Bi-2223 filament and the solder, similar to the aforedescribed Bi-2212 soldering [109], was not discussed. Therefore, current decay measurements for a closed loop sample might be necessary to prove the formation of a superconducting joint with an ultra-low R_j.

The possibility of formation of a superconducting joint between an HTS conductor and a superconducting solder has not been sufficiently discussed. Therefore, it is not clear whether the supercurrent can transfer from LTS to HTS with a high J_c, despite the different superconducting symmetry of the LTS (*s*-wave) and HTS (*d*-wave). Furthermore, there is considerable room for improvement in the fabrication conditions to from the superconducting joint using the superconducting solder. The solder's corrosion or formation of a thin insulator at the HTS surface can be suppressed through heat treatment at relatively lower temperatures. The solder can be optimized to form the superconducting joint between an HTS conductor and a solder.

3.5.2 Low resistive joint for HTS conductors. Banno et al. reported the difficulties in forming the superconducting joint between the REBCO CC and NbTi conductor [48]. Consequently, the compact "boat-type" joint structure with a reduced joint resistance between the REBCO CC and NbTi conductor was reported, as shown in Figure 19. After the REBCO CC was rolled into a metal boat, the superconducting solder was poured into the boat, and the LTS superconducting

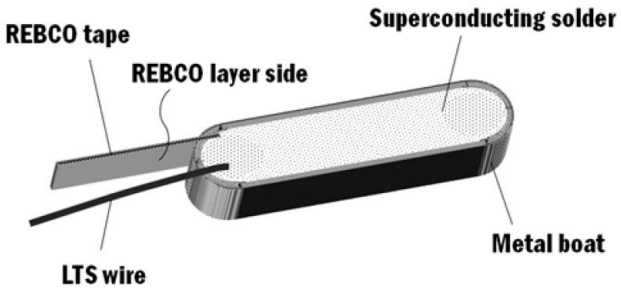

Figure 19. Schematic of a boat-type joint between a REBCO CC and a NbTi wire. Figure adapted from [48]. (IOP publishing, 2020).

joint was formed using the matrix-replacement method between the NbTi wire and the superconducting solder. The joint resistance was reduced to 0.7 nΩ at 4.2 K and 0.4 T by embedding a 2-m-long REBCO CC. Bruker-BioSpin GmbH [34] suggested a soldered lap joint between LTS and HTS conductors wound as a coil, which was also formed a sufficiently compact joint structure.

Several low resistive joining methods such as Sn–Pb soldering [111], mechanical joint (pressure welding) with In foil inserts [112][113], hybrid welding combined with ultrasonic welding and In–Sn solder infiltration [114][115], and ultrasonic welding with In foil inserts [113][116], have been developed for HTS conductors of REBCO CCs and Bi-2223/Ag tapes. A joint resistivity (product of the joint resistance and joint area) of ~15–50 nΩ cm^2 at 77 K in self-field was achieved. At 4.2 K, under magnetic fields less than 1 T, the joint resistivity of the soldering was less than half compared with that at 77 K in self-field [117]. Therefore, using the joining methods described before, a joint resistivity less than 10 nΩ cm^2 can be achieved, indicating that the joint length can be shortened to achieve a sufficiently low resistance compared to that shown in Table 1 (~40 nΩ cm^2). A practical joint showing substantially low resistance might be achievable using the aforementioned joining methods and a compact joint structure [34][48].

There are several advantages of the resistive joining methods. First, the time required to fabricate the resistive joints is short (within several minutes or hours) compared to that required for the formation of HTS superconducting joints. Additionally, they are highly reliable, exhibit high mechanical robustness, and have good reproducibility. Owing to these advantages, the resistive joining methods have been extensively used in various superconducting applications. Therefore, the resistive joining method is a better choice for developing HTS magnets, if the self-inductance of a magnet is sufficiently high or the temporal field stability is not essential.

3.6 Summary, future prospects, and issues to be addressed pertaining to the HTS superconducting joint technology. The recent developments in HTS superconducting joint technology were reviewed. The HTS–HTS superconducting joints and HTS–LTS resistive joints are summarized in Table 2. The superconducting joints exhibiting high I_{cj} (~10^2 A) and ultra-low R_j (< 10^{-11} Ω) for REBCO CCs, Bi-2223 tapes and Bi-2212 wires were successfully demonstrated. The implementation of the HTS superconducting joints in LTS/HTS NMR magnets has progressed. The superconducting joint technology for producing joints between HTS and LTS conductors should be developed further. Additionally, reliable low resistive joining methods for the HTS conductors were investigated.

Based on these backgrounds, several issues have still remained to be addressed in the HTS superconducting joint technology for ultra-high field persistent-mode magnets. The primary issues are as follows:

(1) Criterion for I_{cj}: The I_{cj} criterion has not been determined to date, and the general criterion of 1 μV or 1 μV cm^{-1} is inadequate as the corresponding R_j is significantly large. For example, if we assume I_{cj} as 1000 A under the 1 μV criterion, the corresponding R_j would be 10^{-9} Ω. Measuring the I_{cj} from the *V*–*I* measurement values under the ultra-low R_j criterion of less than 10^{-11} Ω is not feasible. The power-*n* model is often used to fit a *V*–*I* curve because I_{cj} can be estimated in an ultra-low voltage region of less than 1 nV. However, it is reported that the power-*n* model works well in a limited voltage region [118]. Therefore, the estimated I_{cj} in the ultra-low voltage region is not always precise. Further discussion is necessary to determine the criterion for I_{cj}.

(2) Mechanical strength and reinforcement: The mechanical strength of the joint is essential for the application to magnets operated in the persistent-mode. Thus, it is important to discuss the required mechanical strength and the reinforcement method. Because the direction of the current often changes through the joint part, the electromagnetic force may produce a complex mechanical stress on the superconducting joint under an external field. Reportedly, mechanical failure such as shear, cleavage, and peeling failure occur frequently in the REBCO CCs [119]; thus, such mechanical failures can also occur in the REBCO superconducting joints. Furthermore, the Bi-2223 and Bi-2212 superconducting joints are also easily degraded by mechanical stress because of their brittleness in the absence of reinforcements. However, sufficiently improving the mechanical strength of the HTS superconducting joint by optimizing the joining conditions can be difficult. This is because the conductors around the joint part, in which the superconducting layers are exposed, are usually brittle. Thus, other remedies are required to maintain the sufficient mechanical strength of the joints. Mechanical reinforcement might be effective such as embedding a joint in bulk of the solder or resin. However, any degradation in the joint due to such a reinforcement should be investigated.

(3) Joints applicable for high field magnets and generating a high magnetic field in the persistent-mode: A large number of the short joint samples have been fabricated. However, only a few reports on the joints between terminal conductors of a practical magnet have been published. Therefore, fabrication of such joints and generation of a stable high field should be attempted, which is crucial for applying the superconducting joints to the practical ultra-high field persistent-mode magnets. An improved joining process particularly for the terminal conductors may need to be established.

(4) Establishing on-site joining methods: Considering the superconducting joints for LTS magnets are routinely performed at the manufacturing site, such on-site joining methods with high reproducibility should be established for HTS conductors as well. Because the HTS joining methods comprise multiple and complex steps, it would be beneficial to reduce the steps in the process or apply automatic processing. Furthermore, on-site evaluation methods might need to be established for the I_{cj} and R_j of the HTS superconducting joints.

Issue (1) is crucial to advance further in the field of HTS superconducting joint technology. However, issues (2), (3), and (4) are essential for applying the HTS superconducting joint to practical persistent-mode magnets. By addressing these issues, the HTS superconducting joint technology can mature as the HTS magnet technology, thereby leading to the implementation of the superconducting joints in ultra-high field persistent-mode HTS magnets for NMR and MRI applications in the future.

Other than the temporal magnetic field stability, the operating magnets in the persistent-mode have several advantages as compared with those operating in the driven mode. First, the consumption of electrical energy is substantially low without a power supply. Second, an operation expert is not always needed during the persistent-mode operation. Furthermore, the heat leaks can be reduced without current leads. Finally, the robustness against power outage is relatively high. Owing to these advantages, almost all the practical LTS magnet systems are operated in the persistent-mode using superconducting joints. Therefore, the development of HTS superconducting joint technology must advance towards the widespread application of HTS magnet systems operated in the persistent-mode.

4. Summary

(1) The magnetic field of high-field NMR and MRI magnets requires temporal stability. Therefore, LTS NMR and MRI

Table 2. Comparison of the HTS–HTS and HTS–LTS joint technologies.

		REBCO	Bi-2223	Bi-2212	HTS-LTS
High I_{cj} (~10^2 A)	at 4.2 K	✓	✓	✓	–
	at > 20 K	✓	✓	–	–
Ultra-low R_j (< 10^{-11} Ω)	at 4.2 K	✓	✓	✓	–
	at > 20 K	✓	Few data	–	–
Implementation of the joint technology in a persistent-mode LTS/HTS NMR magnet		✓ Drift rate: ~0.03 ppb/h, R_j: < 10^{-14} Ω (4.2 K, 0.2–0.6 T)	Termination of an insert coil. (R_j of ~10^{-12} Ω at 4.2 K in stand-alone test)	–	–
Comment		Several methods were proposed. Development of the iGS joint has been advanced.	Two methods were proposed. An improved coil joining process is needed.	Joints using unreacted wires were proposed. Reproducibility seems to be high.	Various low resistive joining methods were developed. (~15–50 nΩ cm^2 at 77 K, self-field)

magnets are usually operated in the persistent current mode (persistent-mode), for which high-performance LTS superconducting joints are developed by various manufacturers.

(2) An HTS inner coil and LTS outer coil must be used to achieve an ultra-high field NMR magnet of > 23.5 T (1 GHz for ^{1}H NMR). To date, such a magnet has been operated in the driven mode, because the HTS superconducting joint has not been established. However, considerable progress has been made in the last decade in the superconducting joint technology for HTS conductors. Therefore, ultra-high field persistent-mode LTS/HTS NMR magnets and HTS MRI magnets are no longer a dream.

(3) Herein, we first review the temporal drift and fluctuations in the magnetic field for driven mode NMR and MRI magnets with HTS coils. Furthermore, we discuss adequate methods for stabilizing the temporal magnetic field fluctuations.

(4) We conclude that the best approach to achieve a temporally stabilized magnetic field is by using a superconducting magnet operated in the persistent-mode. The superconducting joint technology for HTS conductors is crucial for developing ultra-high field persistent-mode magnets. Based on this, we reviewed the cutting-edge technologies for developing superconducting joints in HTS conductors.

(5) Recently, the superconducting joint technologies for REBCO CCs, Bi-2223 tapes, and Bi-2212 wires were nearly established. A high joint critical current (~10^2 A) and a sufficiently low joint resistance (< 10^{-11} Ω) were achieved.

(6) Based on the superconducting joint technology, a 9.39 T (400 MHz) persistent-mode LTS/REBCO NMR magnet was developed. The superconducting joints (the iGS joints) between the REBCO CCs showed a reasonable performance, resulting in the generation of an extremely stable magnetic field. This indicates that the HTS superconducting joint technology can be extended further.

(7) Despite these results, several issues in superconducting joint technology need to be addressed. The primary issues are development of HTS–LTS superconducting joints, adequate joint critical current criteria, mechanical strength and reinforcement of joints, superconducting joint applicable for coils of practical HTS magnets, generating a stable high field in the persistent-mode, and establishing on-site joining methods with high reproducibility. Addressing these issues can lead to the implementation of superconducting joints in ultra-high field persistent-mode magnets in the future, which will be used for NMR and MRI systems.

Acknowledgements

This work was supported by JST Mirai Program Grant Number JPMJMI17A2.

References

[1] https://www.conectus.org/market.html (accessed August 2021)
[2] A E Derome 1987 *Modern NMR Techniques for Chemistry Research* (Oxford, UK: Pergamon Press)
[3] Brittles G D, Mousavi T, Grovenor C R M, Aksoy C and Speller S C 2015 Persistent current joints between technological superconductors *Supercond. Sci. Technol.* **28** 093001
[4] Liu J, Cheng J, Feng Z, Wang Q, Kun C and Xian L 2013 Electrical properties of cold-pressing welded NbTi persistent joints *Cryogenics* **58** 62–67
[5] Kodama M, Okamoto K, Koga Y, Yamamoto T and Watanabe H 2015 Analysis for formation of current path in the superconducting joint between Nb-Ti wires with the solder matrix replacement method *Supercond. Sci. Technol.* **28** 045019

[6] Becker E D 1993 A brief history of nuclear magnetic resonance *Anal. Chem.* **65** 295A–302A

[7] Wilson M N 2012 A Century of superconducting technology *AIP Conf. Proc.* **1435** 11–35

[8] Nelson F A and Weaver H E 1964 Nuclear magnetic resonance spectroscopy in superconducting magnetic fields *Science* **146** 223–232

[9] Nuding J M 1969 Method of making a superconductive joint *US Patent* 3422529

[10] Teodorescu R 2015 NMR Magnets: A Historical Overview *Modern NMR Approaches to the Structure Elucidation of Natural Products* 26–37 (Cambridge, UK: The Royal Society of Chemistry)

[11] Cosmus T C and Parizh M 2011 Advances in Whole-Body MRI Magnets *IEEE Trans. Appl. Supercond.* **21** 2104–2109

[12] Godeke A, Jewell M C, Fischer C M, Squitieri A, Lee P J and Larbalestier D C 2005 The upper critical field of filamentary Nb_3Sn conductors *J. Appl. Phys.* **97** 093909

[13] Thornton R F 1986 Superconducting joint for superconducting wires and coils and method of forming *US Patent* 4744506

[14] https://ir.bruker.com/press-releases/press-release-details/2009/Worlds-First-1000-MHz-NMR-Spectrometer-Now-Offers-New-Research-Capabilities-to-European-Scientists-Following-its-Successful-Installation-at-CRMN-in-Lyon-France/default.aspx (accessed August 2021)

[15] Larbalestier D C, Jiang J, Trociewitz U P, Kametani F, Scheuerlein C, Dalban-Canassy M, Matras M, Chen P, Craig N C, Lee P J and Hellstrom E E 2014 Isotropic round-wire multifilament cuprate superconductor for generation of magnetic fields above 30 T *Nat. Mater.* **13** 375–381

[16] Uglietti D 2019 A review of commercial high temperature superconducting materials for large magnets: from wires and tapes to cables and conductors *Supercond. Sci. Technol.* **32** 053001

[17] Berrospe-Juarez E, Zermeño V M R, Trillaud F, Gavrilin A V, Grilli F, Abraimov D V, Hilton D K and Weijers H W 2018 Estimation of Losses in the (RE)BCO Two-Coil Insert of the NHMFL 32 T All-Superconducting Magnet *IEEE Trans. Appl. Supercond.* **28** 4602005

[18] Liu J, Wang Q, Qin L, Zhou B, Wang K, Wang Y, Wang L, Zhang Z, Dai Y, Liu H, Hu X, Wang H, Cui C, Wang D, Wang H, Sun J, Sun W and Xiong L 2020 World record 32.35 tesla direct-current magnetic field generated with an all-superconducting magnet *Supercond. Sci. Technol.* **33** 03LT01

[19] Suetomi Y, Yoshida T, Takahashi S, Takao T, Nishijima G, Kitaguchi H, Miyoshi Y, Hamada M, Saito K, Piao R, Takeda Y, Maeda H and Yanagisawa Y 2021 Quench and self-protecting behaviour of an intra layer no-insulation (LNI) REBCO coil at 31.4 T *Supercond. Sci. Technol.* **34** 064003

[20] Yanagisawa Y, Nakagome H, Tennmei K, Hamada M, Yoshikawa M, Otsuka A, Hosono M, Kiyoshi T, Takahashi M, Yamazaki T and Maeda H 2010 Operation of a 500 MHz high temperature superconducting NMR: Towards an NMR spectrometer operating beyond 1 GHz *J. Magn. Reson.* **203** 274–282

[21] Yanagisawa Y, Nakagome H, Hoshino M, Hamada M, Kiyoshi T, Hobo F, Takahashi M, Yamazaki T and Maeda H 2008 Towards beyond-1 GHz solution NMR: internal ^2H lock operation in an external current mode *J. Magn. Reson.* **192** 329–337

[22] Hashi K, Ohki S, Matsumoto S, Nishijima G, Goto A, Deguchi K, Yamada K, Noguchi T, Sakai S, Takahashi M, Yanagisawa Y, Iguchi S, Yamazaki T, Maeda H, Tanaka R, Nemoto T, Suematsu H, Miki T, Saito K and Shimizu T 2015 Achievement of 1020 MHz NMR *J. Magn. Reson.* **256** 30–33

[23] Hashi K, Deguchi K, Yamazaki T, Ohki S, Matsumoto S, Nishijima G, Goto A, Yamada K, Noguchi T, Sakai S, Takahashi M, Yanagisawa Y, Iguchi S, Maeda H, Tanaka R, Nemoto T, Suematsu H, To J, Torres J, Pervushin K and Shimizu T 2016 Efficiency of High Magnetic Fields in Solid-state NMR *Chem. Lett.* **45** 209–210

[24] Bascuñán J, Hahn S, Park D K and Iwasa Y 2011 A 1.3-GHz LTS/HTS NMR Magnet—A progress report *IEEE Trans. Appl. Supercond* **21** 2092–2095

[25] Lee H, Park Y J, Kim K L, Choi Y H, Yang D G 2013 Superconducting joint of 2G ReBCO coated conductors *International Conference on Magnet Technology (Boston, USA)*

[26] Park Y, Shin H-J, Kim Y-G, Oh Y K and Lee H 2013 Effects of melting diffusion and annealing in oxygen on superconducting characteristics of GdBCO Coated conductors: preliminary results *IEEE Trans. Appl. Supercond.* **23** 6600804

[27] Park Y, Lee M, Ann H, Choi Y H and Lee H 2014 A superconducting joint for $GdBa_2Cu_3O_{7-\delta}$-coated conductors, *NPG Asia Mater.* **6** e98

[28] Park Y J, Lee M W, Oh Y K and Lee H G 2014 Laser drilling: enhancing superconducting joint of $GdBa_2Cu_3O_{7-\delta}$ coated conductors *Supercond. Sci. Technol.* **27** 085008

[29] Ohki K, Nagaishi T, Kato T, Yokoe D, Hirayama T, Ikuhara Y, Ueno T, Yamagishi K, Takao T, Piao R, Maeda H and Yanagisawa Y 2017 Fabrication, microstructure and persistent current measurement of an intermediate grown superconducting (iGS) joint between REBCO-coated conductors *Supercond. Sci. Technol.* **30** 115017

[30] Takeda Y, Motoki T, Kitaguchi H, Nakashima T, Kobayashi S, Kato T and Shimoyama J 2019 High I_c superconducting joint between Bi2223 tapes *Appl. Phys. Express* **12** 023003

[31] Yanagisawa Y, Piao R, Suetomi Y, Yamazaki T, Yamagishi K, Ueno T, Takao T, Ohki K, Yamaguchi T, Nagaishi T, Kitaguchi H, Miyoshi Y, Yoshikawa M, Hamada M, Saito K, Hachitani K, Ishii Y and Maeda H 2021 Development of a persistent-mode NMR magnet with superconducting joints between high-temperature superconductors *Supercond. Sci. Technol.* **34** 115006

[32] Maeda H, Shimoyama J, Yanagisawa Y, Ishii Y and Tomita M 2019 The MIRAI Program and the New Super-High Field NMR Initiative and Its Relevance to the Development of Superconducting joints in Japan *IEEE Trans. Appl. Supercond.* **29** 4602409

[33] https://www.bruker.com/ja/news-and-events/news/2020/successful-installation-of-worlds-first-12-ghz-nmr-system-enables-novel-functional-structural-biology-research.html (accessed August 2021)

[34] Roth G and Kasten A, Magnetic 2015 Coil Assembly, Comprising an HTS Strip Conductor and an LTS Wire, Which Form a Joint *WO Patent 2015049358*

[35] Sinanna A, Aguiar P M, d'Amico F, Bermond S, Bredy P, Donati A, Hugon C, Lannou H, Sakellariou D, Schild T, and Tixador P 2010 Field Stabilization of the Iseult/Inumac Magnet Operating in Driven Mode *IEEE Trans. Appl. Supercond.* **20** 790–793

[36] Gan Z, Hung I, Wang X, Paulino J, Wu G, Litvak I M, Gor'kov P L, Brey W W, Lendi P, Schiano J L, Bird M D, Dixon I R, Toth J, Boebinger G S and Cross T A 2017 NMR spectroscopy up to 35.2 T using a series-connected hybrid magnet *J. Magn. Reson.* **284** 125–136

[37] Bird M D, Bai H, Dixon I R and Gavrilin A V 2019 Test Results of the 36 T, 1 ppm Series-Connected Hybrid Magnet System at the NHMFL *IEEE Trans. Appl. Supercond.* **29** 4300105

[38] Koyama Y, Takao T, Yanagisawa Y, Nakagome H, Hamada M, Kiyoshi T, Takahashi M, and Maeda H 2009 Towards beyond 1 GHz NMR: Mechanism of the long-term drift of screening current-induced magnetic field in a Bi-2223 coil *Physica C* **469** 694-701

[39] Yanagisawa Y, Piao R, Iguchi S, Nakagome H, Takao T, Kominato K, Hamada M, Matsumoto S, Suematsu H, Jin X, Takahashi M, Yamazaki T and Maeda H 2014 Operation of a 400 MHz NMR magnet using a (RE: rare earth)$Ba_2Cu_3O_{7-x}$ high-temperature superconducting coil: Towards an ultra-compact super-high field NMR spectrometer operated beyond 1 GHz *J. Magn. Reson.* **249** 38–48.

[40] Takahashi M, Ebisawa Y, Tennmei K, Yanagisawa Y, Hosono, M, Takasugi, K, Hase T, Miyazaki T, Fujito T, Nakagome H, Kiyoshi T, Yamazaki T and Maeda H 2012 Towards a beyond 1 GHz solid-state nuclear magnetic resonance: external lock operation in an external current mode for a 500 MHz nuclear magnetic resonance *Rev. Sci. Instrum.* **83** 105110

[41] Terao Y, Ozaki O, Ichihara C, Kawashima S, Hase T, Kitaguchi H, Kobayashi S, Sato K, Nakajima I, Oonishi N, Poole M, Takeda K, Urayama S, and Fukuyama H 2013 Newly designed 3 T MRI magnet wound with Bi-2223 tape conductors *IEEE Trans. Appl. Supercond.* **23** 4400904

[42] Yokoyama S, Miura H, Matsuda T, Inoue T, Morita Y, Eguchi R, Otake S, Tanabe H, Sato S, Kiss T, Miyagi D, Tsuda M, Nakamura T and Shirai Y 2020 Design and Cooling Properties of High Stable Field REBCO Superconducting Magnet for MRI *IEEE Trans. Appl. Supercond.* **30** 4400904

[43] Kitada S, Sakamoto R, Shirai Y, and Yokoyama S 2020, Feedforward current control of MRI magnet with power supply driven operation *J. Phys.: Conf. Ser.* **1559** 012123

[44] Kiyoshi T, Sato A, Takeuchi T, Itoh K, Matsumoto S, Ozaki O, Fukushima K, Wada H, Yoshikawa M, Kamikado T, Ito S, Miki T, Hase T, Hamada M, Hayashi S, Kawate Y and Hirose R 2002 Persistent-Mode Operation of a 920 MHz High-Resolution NMR Magnet *IEEE Trans. Appl. Supercond.* **12** 711–714.

[45] Kiyoshi T, Maeda H, Kikuchi J, Ito Y, Hirota H, Yokoyama S, Ito S, Miki T, Hamada M, Ozaki O, Hayashi S, Kurihara N, Suematsu H, Yoshikawa M, Matsumoto S, Sato A and Wada H 2004 Present Status of 920 MHz High-Resolution NMR Spectrometers *IEEE Trans. Appl. Supercond.* **14** 1608–1612

[46] Iwasaki S, Investigation on the low resistance normal conducting joint between YBCO conductors, Master's thesis, Sophia University, Japan (2012)

[47] Takahashi S, Suetomi Y, Takao T, Yanagisawa Y, Maeda H, Takeda Y, and Shimoyama J 2020 Hoop stress modification, stress hysteresis and degradation of a REBCO coil due to the screening current under external magnetic field cycling *IEEE Trans. Appl. Supercond.* **30** 4602607

[48] Banno N, Asano T, Kato T and Maeda H 2020 A new concept for developing a compact joint structure for reducing joint resistance between high-temperature superconductors (HTS) and low-temperature superconductors (LTS) *Supercond. Sci. Technol.* **32** 053001

[49] https://indico.cern.ch/event/445667/ (accessed August 2021)

[50] https://indico.cern.ch/event/763185/ (accessed August 2021)

[51] https://www.ascinc.org/asc2018/wp-content/uploads/2018/11/ASC2018_ProgramBook.pdf (accessed August 2021)

[52] Kobayashi K, Nishijima G, Uchida A, Amaya M, Banno N and Kitaguchi H 2020 Development of a Superconducting Joint Resistance Evaluation System *IEEE Trans. Appl. Supercond.* **30** 9000204

[53] Iwasa Y 1976 Superconducting joint between multifilamentary wires 2. Joint evaluation technique *Cryogenics* **16** 217–219

[54] Jorgensen J D, Veal B W, Paulikas A P, Nowicki L J, Crabtree G W, Claus H, and Kwok W K 1990 Structural properties of oxygen-deficient $YBa_2Cu_3O_{7-\delta}$ *Phys. Rev. B* **41** 1863–1877.

[55] Iijima Y, Tanabe N, Kohno O and Ikeno Y 1992 In-plane aligned $YBa_2Cu_3O_{7-x}$ thin films deposited on polycrystalline metallic substrates *Appl. Phys. Lett.* **60** 769–771

[56] Tokudome M, Doi T, Tomiyasu R, Sato S, Hakuraku Y, Kubota S, Shima K, Kashima N and Nagaya S 2008 Fabrication of $YBa_2Cu_3O_7$ thin film on cube-textured Cu tape *J. Appl. Phys.* **104** 103913

[57] Nagaishi T, Shingai Y, Konishi M, Taneda T, Ota H, Honda G, Kato T and Ohmatsu K 2009 Development of REBCO coated conductors on textured metallic substrates *Physica C* **469** 1311–1315

[58] Foltyn S R, Civale L, Macmamus-Driscoll J L, Jia Q X, Maiorov B, Wang H and Maley M 2007 Materials science challenges for high-temperature superconducting wire *Nat. Mater.* **6** 631–642

[59] Hahn S, Kim K, Kim K, Hu X, Painter T, Dixon I, Kim S, Bhattarai K R, Noguchi S, Jaroszynski J and Larbalestier D C 2019 45.5-tesla direct current magnetic field generated with a high-temperature superconducting magnet *Nature* **570** 496–499

[60] Kato T, Yoshida R, Yokoe D, Ohki K, Nagaishi T, Yanagisawa Y, Hirayama T, Ikuhara Y and Maeda H 2020 Nanostructural evolution of intermediate grown superconducting joint layers between $GdBa_2Cu_3O_y$ coated conductors *Supercond. Sci. Technol.* **33** 105008

[61] https://www.furukawa.co.jp/en/release/2016/kenkai_160427.html (accessed August 2021)

[62] Mukoyama S, Nakai A, Sakamoto H, Matsumoto S, Nishijima G, Hamada M, Saito K and Miyoshi Y 2018

Superconducting joint of REBCO wires for MRI magnet *J. Phys.: Conf. Ser.* **1054** 012038

[63] Takahashi K, Hase T, Awaji S, Nakai A, Yamano S, Mukoyama S and Sakamoto H 2018 Performance of an HTS Persistent Current System for REBCO Pancake Coil *IEEE Trans. Appl. Supercond.* **28** 4600104

[64] Matsumoto S, Nishijima G, Nakai A, Sakamoto H, Mukoyama S, Miyoshi Y, Saito K and Hamada M 2019 Estimation of Joint Resistance in REBCO Single-Turn Loop Under Magnetic Fields *IEEE Trans. Appl. Supercond.* **29** 4602005

[65] Nishijima G, Matsumoto S, Nakai A, Sakamoto H, Mukoyama S, Miyoshi Y, Saito K and Hamada M 2019 Transport Property of REBCO Superconducting Joints in Magnetic Fields at Various Temperatures *IEEE Trans. Appl. Supercond.* **29** 4602105

[66] Jin X, Yanagisawa Y, Maeda H and Takano Y 2015 Development of a superconducting joint between a $GdBa_2Cu_3O_{7-\delta}$-coated conductor and $YBa_2Cu_3O_{7-\delta}$ bulk: towards a superconducting joint between RE (Rare Earth) $Ba_2Cu_3O_{7-\delta}$-coated conductors *Supercond. Sci. Technol.* **28** 075010

[67] Shiohara Y and Endo A 1997 Crystal growth of bulk high-T_c superconducting oxide materials *Mater. Sci. Eng. R Rep.* **19** 1–86

[68] Jin X, Yanagisawa Y and Maeda H 2018 Measurement of Persistent Current in a Gd123 Coil With a Superconducting Joint Fabricated by the CJMB Method *IEEE Trans. Appl. Supercond.* **28** 4602604

[69] Jin X, Mawatari Y, Kuzuya T, Amakai Y, Tayu Y, Momono N, Hirai S and Yanagisawa Y 2019 Microstructural Analysis of Superconducting Joint Fabricated Using CJMB Between Gd123-Coated Conductors *IEEE Trans. Appl. Supercond.* **29** 6602205

[70] Hiramatsu K, Teranishi R, Yamada K, Sato Y and Kaneko K 2016 Joint of $REBa_2Cu_3O_{7-\delta}$ Coated Conductors using Metal Organic Deposition *Phys. Proc.* **81** 109–112

[71] Teranishi R, Hiramatsu K, Yasuyama S, Miyajima T, Sato Y, Kaneko K, Awaji S, Matsumoto A and Inoue M 2019 Superconducting Joint of $GdBa_2Cu_3O_y$ Coated Conductors by crystallization of an Additionally Deposited Precursor Layer *IEEE Trans. Appl. Supercond.* **29** 6602904

[72] Miyajima T, Teranishi R, Yasuyama S, Sato Y, Kaneko K, Petrykin V, Lee S, Okada T, Awaji S and Matsumoto A 2019 Influence of joint pressure on superconducting and mechanical properties for jointed $GdBa_2Cu_3O_y$ coated conductors via precursor films *Jpn. J. Appl. Phys.* **58** 050907

[73] Miyajima T, Teranishi R, Yasuyama S, Sato Y, Kaneko K, Maeda T, Ochi M, Hiramatsu K, Nakamura M, Petrykin V, Lee S, Okada T and Awaji S 2019 Microstructures of superconducting joint between $GdBa_2Cu_3O_y$-coated conductors via additionally deposited precursor films *Jpn. J. Appl. Phys.* **58** 050913

[74] Sato K, Kobayashi S and Nakashima T 2012 Present Status and Future Perspective of Bismuth-Based High-Temperature Superconducting Wires Realizing Application Systems *Jpn. J. Appl. Phys.* **51** 010006

[75] Ayai N, Kato T, Fujikami J, Kobayashi S, Kikuchi M, Yamazaki K, Yamade S, Ishida T, Tatamidani K, Hayashi K, Sato K, Hata R, Kitaguchi H, Kumakura H, Osamura K and Shimoyama J 2008 DI-BSCCO wire with I_c over 200 A at 77 K *J. Phys.: Conf. Ser.* **97** 012112

[76] Nakashima T, Kobayashi S, Kagiyama T, Yamazaki K, Kikuchi M, Yamade S, Hayashi K, Sato K, Shimoyama J, Kitaguchi H and Kumakura H 2011 Recent R&D progress on DI-BSCCO wires with high critical current properties *Physica C* **471** 1086–1089

[77] Nishijima G, Matsumoto S, Hashi K, Ohki S, Goto A, Noguchi T, Iguchi S, Yanagisawa Y, Takahashi M, Maeda H, Miki T, Saito K, Tanaka R and Shimizu T 2016 Successful Upgrading of 920-MHz NMR Superconducting Magnet to 1020 MHz Using Bi-2223 Innermost Coil *IEEE Trans. Appl. Supercond.* **26** 4303007

[78] Awaji S, Watanabe K, Oguro H, Miyazaki H, Hanai S, Tosaka T and Ioka S 2017 First performance test of a 25 T cryogen-free superconducting magnet *Supercond. Sci. Technol.* **30** 065001

[79] Tkaczyk J E, Arendt R H, Bednarczyk P J, Garbauskas M F, Jones B A, Kilmer R J and Lay K W 1993 Superconducting joints formed between powder-in-tube $Bi_2Sr_2Ca_2Cu_3O_z$/Ag tapes *IEEE Trans. Appl. Supercond.* **3** 946–948

[80] Kim K T, Kim J H, Joo J and Nash P 2003 Superconducting Joint of Multifilamentary Bi(Pb)-Sr-Ca-Cu-O Tapes *IEEE Trans. Appl. Supercond.* **13** 2996–2999

[81] Wang Y, Luan W Z, Lin W, Hua P W, Li Y N, Feng R B, Zhou Q, Yao Y X, Yuan G S 2003 Superconducting joint on Bi2223/Ag multifilamentary tape *Physica C* **386** 174–178

[82] Guo W, Zou G, Wu A, Wang Y, Bai H and Ren J 2009 Superconducting joint of Bi-2223/Ag superconducting tapes by diffusion bonding *Physica C* **469** 1898–1901

[83] Guo W, Zou G, Wu A, Zhou F and Ren J 2010 Fabrication of joint Bi-2223/Ag superconducting tapes with BSCCO superconducting powders by diffusion bonding *Physica C* **470** 440–443

[84] Ebara Y, Morie T, Nishine K and Tsurudome T 2017 Electrical Resistance Measurement Method to Investigate Superconducting Joints in Bi-2223 Tape *IEEE Trans. Appl. Supercond.* **27** 9000904

[85] Ebara Y, Tsurudome T, Morie T, Nishine K, Oguro H and Awaji S 2018 Experimental Investigation of Bi-2223/Ag Superconducting Tape Joints *IEEE Trans. Appl. Supercond.* **28** 6400203

[86] Ishizuka M and Sakuraba J 2006 Critical current density (J_c) and mechanical characteristics of a Bi-2223 bulk current lead for cryocooler-cooled superconducting magnets *Physica C* **433** 173–181

[87] Jin X, Suetomi Y, Piao R, Matsutake Y, Yagai T, Mochida H, Yanagisawa Y and Maeda H 2019 Superconducting joint between multi-filamentary $Bi_2Sr_2Ca_2Cu_3O_{10+\delta}$ tapes based on incongruent melting for NMR and MRI applications *Supercond. Sci. Technol.* **32** 035011

[88] Komatsu H, Kato Y, Miyashita S, Inoue T and Hayashi S 1991 In situ observations of crystal growth of Bi-based oxide superconductors *Physica C* **190** 14–17

[89] Suzuki T, Yumoto K, Mamiya M, Hasegawa M and Takei H 1998 A phase diagram of the $Bi_2Sr_2CuO_6$–$CaCuO_2$ system in relation to Bi-based superconductors *Physica C* **301** 173–184

[90] Shimoyama J, Tanimoto A, Makise T, Yamamoto A, Katsura Y, Iwayama I, Horii S, Kishio K, Kato T, Kobayashi S, Yamazaki K, Hayashi K and Sato K 2007 How to improve critical current properties of Bi2223 and MgB_2 tapes *Physica C* **463-465** 802–806

[91] Obata K, Shimoyama J, Yamamoto A, Ogino H, Kishio K, Kobayashi S and Hayashi K 2012 Critical Current Properties of *c*-Axis Oriented Bi(Pb)2223 Bulks Sintered under High Gas Pressures *Phys. Proc.* **36** 665–668

[92] Tajima R, Shimoyama J, Yamamoto A, Ogino H, Kishio K, Nakashima T, Kobayashi S and Hayashi K 2013 Synthesis of Bi2223 by Low P_{O2} Sintering *IEEE Trans. Appl. Supercond.* **23** 6400604

[93] Takeda Y, Shimoyama J, Motoki T, Kishio K, Nakashima T, Kagiyama T, Kobayashi S and Hayashi K 2017 Fabrication of Bi2223 bulks with high critical current properties sintered in Ag tubes *Physica C Supercond.* **534** 9–12

[94] Takeda Y, Shimoyama J, Motoki T, Nakamura S, Nakashima T, Kobayashi S and Kato T 2018 Development of high J_c Bi2223/Ag thick film materials prepared by heat treatment under low P_{O2} *Supercond. Sci. Technol.* **31** 074002

[95] Takeda Y, Motoki T, Kobayashi K, Uchida A, Kitaguchi H, Nakamura S, Matsutake Y, Takahashi S, Yagai T, Takao T, Suetomi Y, Piao R, Yanagisawa Y, Nakashima T, Kobayashi S, Kato T and Shimoyama J 2019 Superconducting joints between Bi2223/Ag tapes towards persistent current HTS magnets *International Conference on Magnet Technology (Vancouver, Canada)*

[96] Kobayashi K, Uchida A, Nishijima G, Takeda Y, Shimoyama J and Kitaguchi H 2020 In-field property of Bi2223 superconducting joint at various temperatures *Applied Superconductivity Conference (Virtual)*

[97] Yamazaki K, Kagiyama T, Kikuchi M, Yamade S, Nakashima T, Kobayashi S, Osabe G, Fujikami J, Hayashi K and Sato K 2012 Recent progress on improvement to mechanical properties of DI-BSCCO wire *Supercond. Sci. Technol.* **25** 054015

[98] Takeda Y, Matsutake Y, Yagai T, Suetomi Y, Piao R, Yanagisawa Y, Kobayashi K, Uchida A, Kitaguchi H, Nakashima T, Kobayashi S, Kato T, Motoki T and Shimoyama J 2020 Superconducting joints between high-strength Bi2223/Ag tapes with reinforcement materials towards persistent-current HTS magnets *Applied Superconductivity Conference (Virtual)*

[99] Kanazawa S and Yanagisawa Y 2019 Superconducting joint interface for multi-filamentary Bi2223 tapes fabricated by JIM method *J. Alloys Compounds* **806** 897–900

[100] Shimoyama J, Kase J, Morimoto T, Mizusaki J and Tagawa H 1991 Oxygen Nonstoichiometry and Phase Instability of $Bi_2Sr_2CaCu_2O_{8+\delta}$ *Physica C* **185–189** 931–932

[101] Kanazawa S 2021 Improvement of Critical Current in Superconducting Joint Between Multi-Filamentary Bi2223 Tapes *IEEE Trans. Appl. Supercond.* **31** 7000104

[102] Tosaka T, Kuriyama T, Yamaji M, Kuwano K, Igarashi M and Terai M 2004 Development of a persistent current switch for HTS magnets *IEEE Trans. Appl. Supercond.* **14** 1218–1221

[103] Weijers H W, Trociewitz U P, Marken K, Meinesz M, Miao H and Schwartz J 2004 The generation of 25.05 T using a 5.11 T Bi2Sr2CaCu2Ox superconducting insert magnet *Supercond. Sci. Technol.* **17** 636–44

[104] Iwasa Y 2017 Towards liquid-helium-free, persistent-mode MgB_2 MRI magnets: FBML experience *Supercond. Sci. Technol.* **30** 053001

[105] Godeke A, Acosta P, Cheng D, Dietderich D R, Mentink M G T, Prestemon S O, Sabbi G L, Meinesz M, Hong S, Huang Y, Miao H and Parrell J 2010 Wind-and-react Bi-2212 coil development for accelerator magnets *Supercond. Sci. Technol.* **23** 034022

[106] Chen P, Trociewitz U P, Davis D S, Bosque E S, Hilton D K, Kim Y, Abraimov D V, Starch W L, Jiang J, Hellstrom E E and Larbalestier D C 2017 Development of a persistent superconducting joint between Bi-2212/Ag-alloy multifilamentary round wires *Supercond. Sci. Technol.* **30** 025020

[107] Trociewitz U P, Chen P, Hilton D K, Abraimov D V, Starch W L, Larbalestier D C, Jiang J, Hellstrom E E, Bosque E S and Matras M 2016 Superconducting joint for high-temperature superconducting BiSrCaCuO(Bi-2212) wire *US Patent* 9966167

[108] Mousavi T, Santra S, Melhem Z, Speller S and Grovenor C 2021 Superconducting Joint Structures For Bi-2212 Wires Using a Powder-in-Tube Technique *IEEE Trans. Appl. Supercond.* **31** 6400504

[109] Mousavi T, Davies T, Melhem Z, Grovenor C R M and Speller S C 2018 Development of Superconducting Soldered Joints Between Bi-2212/Ag Wires *IEEE Trans. Appl. Supercond.* **28** 6400303

[110] Matsumoto R, Iwata H, Yamashita A, Hara H, Nishijima G, Tanaka M, Takeya H and Takano Y 2017 Superconducting joins using Bi-added PbSn solders *Appl. Phys. Express* **10** 093012

[111] Baldan C A, Oliveira U R, Shigue C Y, and Filho E R 2009 Evaluation of Electrical Properties of Lap Joints for BSCCO and YBCO Tapes *IEEE Trans. Appl. Supercond.*, **19** 2831–2834

[112] Nishio T, Ito S, Yusa N, and H. Hashizume 2016 Reducing Joint Resistance by Heat Treatment During Fabrication of a Mechanical Joint of High–Temperature Superconducting Conductors *IEEE Trans. Appl. Supercond.* **26** 4800505

[113] Ito S, Fujii H T, Hayasaka R, Sato Y S and Hashizume H 2019 Comparison of heat assisted lap joints of high-temperature superconducting tapes with inserted indium foils *IEEE Trans. Appl. Supercond.* **29** 6600405

[114] Shin H-S and Kim J-M 2016 Development of Low-Resistance Splice Joint for Long GdBCO Coated Conductor Tapes Using Ultrasonic Welding Method *IEEE Trans. Appl. Supercond.* **26** 6601704

[115] Shin H-S, Kim J-M, and Dedicatoria M J 2016 Pursuing low joint resistivity in Cu-stabilized $REBa_2Cu_3O_\delta$ coated conductor tapes by the ultrasonic weld-solder hybrid method *Supercond. Sci. Technol.* **29** 015005

[116] Ito S, Hayasaka R, Yuki K, Sato Y S and Hashizume H 2020 Joining condition dependency of joint resistance in ultrasonic welding of high-temperature superconducting tapes with indium *J. Phys.: Conf. Ser.* **1559** 012065

[117] Piao R, Miyoshi Y, Yoshikawa M, Saito K, Hamada M, Matsumoto S, Suematsu H, Mochida H, Takao T, Suetomi Y, Takahashi M, Maeda H and Yanagisawa Y 2019 Design and Development of a Compact 1 GHz (23.5 T)-Class NMR Magnet With Bi-2223 Inner Coils *IEEE Trans. Appl. Supercond.* **29** 4300407

[118] Kiss T, Inoue M, Kuga T, Ishimaru M, Egashira S, Irie S, Ohta T, Imamura K, Yasunaga M, Takeo M, Matsushita T, Iijima Y, Kakimoto K, Saitoh T, Awaji S, Watanabe K and Shiohara Y 2003 Critical current properties in HTS tapes *Physica C* **392–396** 1053–1062

[119] Maeda H and Yanagisawa Y 2014 Recent Developments in High-Temperature Superconducting Magnet Technology (Review) *IEEE Trans. Appl. Supercond.* **24** 4602412